NSTX

Supported by U.S. DEPARTMENT OF ENERGY | Office of Science

Liquid Lithium Divertor surface temperature dynamics and edge plasma modification under plasma-induced heating and lithium pre-heating

College W&M
Colorado Sch Mines
Columbia U
CompX
General Atomics
INEL
Johns Hopkins U
LANL
LLNL
Lodestar
MIT
Nova Photonics
New York U
Old Dominion U
ORNL
PPPL
PSI
Princeton U
Purdue U
SNL
Think Tank, Inc.
UC Davis
UC Irvine
UCLA
UCSD
U Colorado
U Illinois
U Maryland
U Rochester
U Washington
U Wisconsin

A. G. McLean Oak Ridge National Laboratory

J.-W. Ahn, T.K. Gray, R. Maingi, M. Bell, R. Bell, M.A. Jaworski, H. Kugel, B.C. Lyons, R.E. Nygren, L. Roquemore, F. Scotti, C.H. Skinner

2nd ISLA
PPPL, April 27, 2011

PPPL Princeton Plasma Physics Laboratory

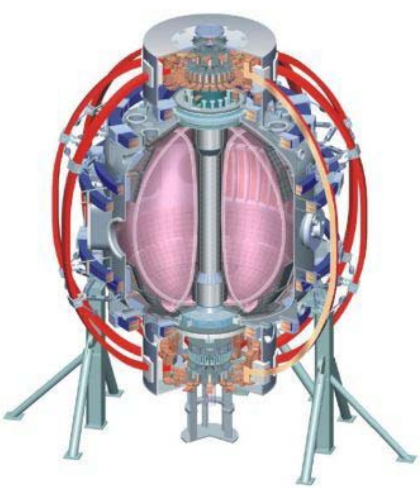

Culham Sci Ctr
U St. Andrews
York U
Chubu U
Fukui U
Hiroshima U
Hyogo U
Kyoto U
Kyushu U
Kyushu Tokai U
NIFS
Niigata U
U Tokyo
JAEA
Hebrew U
Ioffe Inst
RRC Kurchatov Inst
TRINITI
KBSI
KAIST
POSTECH
ASIPP
ENEA, Frascati
CEA, Cadarache
IPP, Jülich
IPP, Garching
ASCR, Czech Rep
U Quebec

Outline

- Dual-band infrared technique demonstrated in NSTX in 2010
- Li melt dynamics on the LLD
- LLD vs. graphite tile surface temperature: Observation of clamping
- Edge plasma modification with and without Li deposition
- Conclusions
- *Time permitting: Thermal diagnostic improvements on NSTX for 2011*

Outline

- Dual-band infrared technique demonstrated in NSTX in 2010
- Li melt dynamics on the LLD
- LLD vs. graphite tile surface temperature: Observation of clamping
- Edge plasma modification with and without Li deposition
- Conclusions

The IR system on NSTX is designed to overcome limitations inherent in a complex Tokamak environment

- Accurate IR measurements are essential for heat load analysis on plasma-facing components (PFCs) during plasma operation, especially in the divertor region
  - Transient heat load can exceed 10 MW/m^2
  - Localize hot spots and significant impurity sources

- Use of lithium coatings in NSTX make assumptions of high surface emissivity inaccurate
  - e.g., ε of graphite >0.85, ε of molten lithium <0.1

- Primary diagnostic effort to move from single-band to dual-band infrared observations
  - Technique measures temperature based on the ratio of integrated IR emission in two IR bands, not single band intensity → Less dependent on emissivity

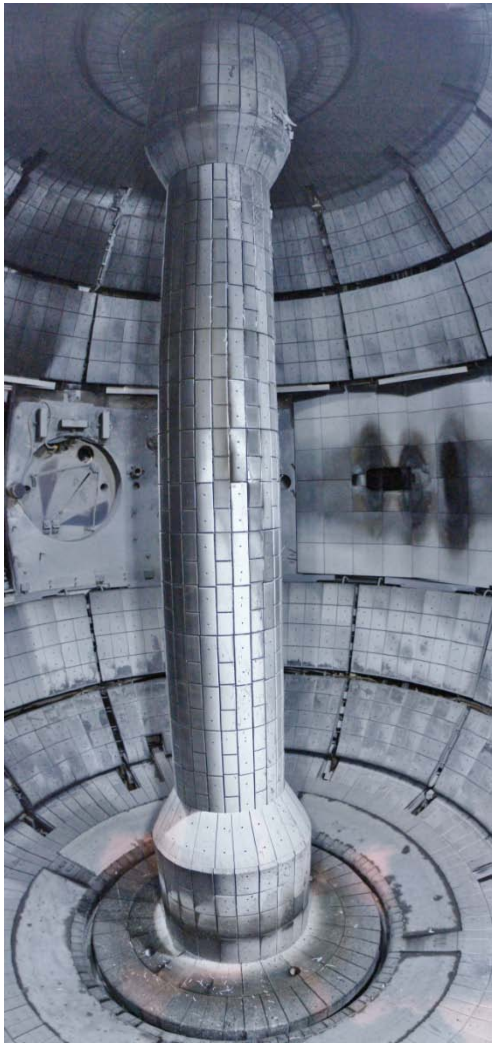

The Liquid Lithium Divertor (LLD) was used extensively in the 2010 NSTX campaign

- Four plates extending toroidally around the outer divertor
- 12, 500W cartridge heaters and 44 type K thermocouples provide active control of each plate's temperature
- Electrically heated to
  - 100-199°C in 7 runs days
  - 200-299°C in 9 run days
  - Up to 320°C in 3 run days
- Heated by repeated plasma discharge exposure to
  - 100-130°C in 3 run days
- Heated by hot forced air to
  - 150-180°C in 2 run days
- Only heating to ≥ 180°C maintained Li as liquid between discharges

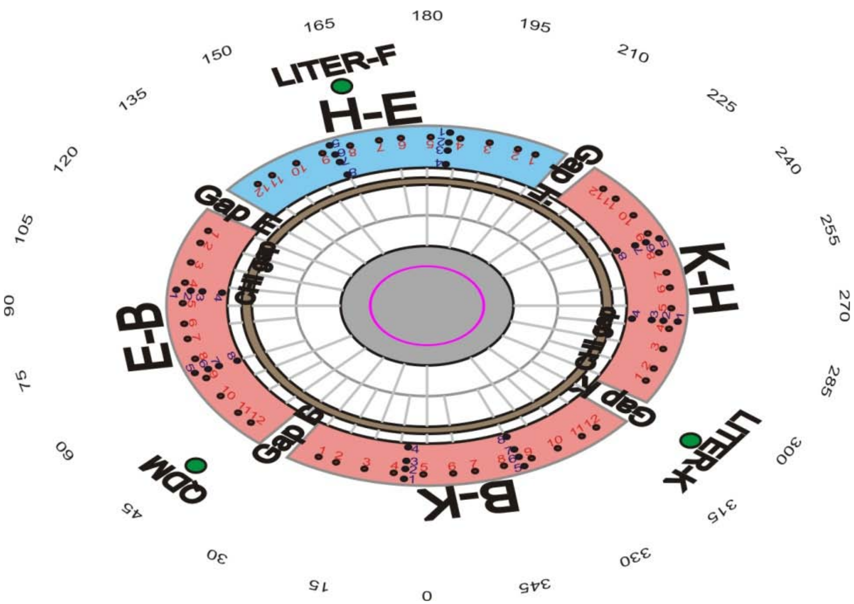

NSTX has extensive infrared coverage for surface temperature and heat flux diagnosis

- Two slow (30 Hz) single-band IR cameras
  - Indigo Omega, 30 Hz, 160x128 pixel uncooled microbolometer FPA, 3.4 x 3.7 x 4.8 cm
  - 7-13 µm, 12-bit, 0-700°C range, ZnSe window
  - 15° FOV of lower divertor, ~0.7 cm/pixel resolution
- One fast (1.6-6.3 kHz) dual-band IR camera
  - Santa Barbara Focal Plane (Lockheed Martin) ImagIR 128x128, 40µm pixel HgCdTe FPA, LN_2-cooled
  - QE>90% from 1.5-11 µm, 14-bit, <20 mK NETD
- 2011 addition of dual-color, wide angle IR camera

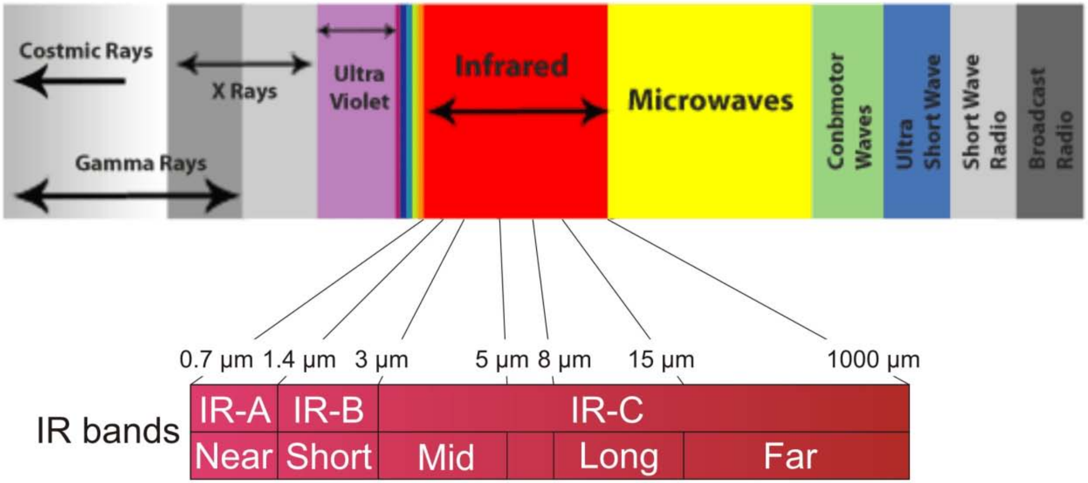

NSTX fast IR camera field of view

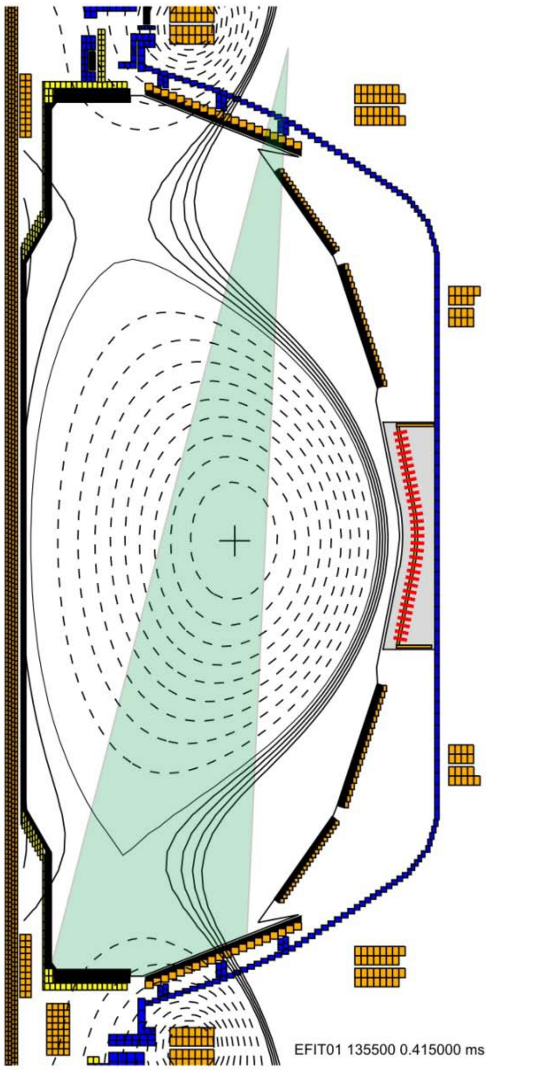

Calibration of the ratio of emission intensities to temperature removes emissivity as a variable

- Two-color camera measures temperature based on the ratio of integrated IR emission in two IR regions, not single band intensity

- Mathematically
  - Planck's law for photon emittance [ph/s/cm²/μm]
  - Radiant emittance from source some fraction of that from a blackbody source [W/cm²/μm]

$$Q_{BB}(\lambda,T) = \frac{2\pi c}{\lambda^4 \cdot \left[exp\left(\frac{hc}{\lambda kT}\right) - 1\right]}$$

$$W(\lambda,T) = \frac{hc}{\lambda} Q(\lambda,T)$$

$$I_{\lambda,surf}(\lambda,\theta,\phi,T) = \varepsilon_{\lambda,\theta}(\lambda,\theta,\phi,T) \cdot I_{\lambda,BB}(\lambda,T)$$

$$\frac{I_{\lambda_1,surf}}{I_{\lambda_2,surf}} = \frac{\varepsilon_{\lambda_1,\theta}}{\varepsilon_{\lambda_2,\theta}} \cdot \frac{I_{\lambda_1,BB}}{I_{\lambda_2,BB}}$$

Calibration of the ratio of emission intensities to temperature removes emissivity as a variable

- Two-color camera measures temperature based on the ratio of integrated IR emission in two IR regions, not single band intensity

- Mathematically
  - Planck's law for photon emittance [ph/s/cm²/μm]
  - Radiant emittance from source some fraction of that from a blackbody source [W/cm²/μm]

$$Q_{BB}(\lambda,T) = \frac{2\pi c}{\lambda^4 \cdot \left[exp\left(\frac{hc}{\lambda kT}\right) - 1\right]} \qquad W(\lambda,T) = \frac{hc}{\lambda} Q(\lambda,T)$$

$$I_{\lambda,surf}(\lambda,\theta,\phi,T) = \varepsilon_{\lambda,\theta}(\lambda,\theta,\phi,T) \cdot I_{\lambda,BB}(\lambda,T)$$

$$\frac{I_{\lambda_1,surf}}{I_{\lambda_2,surf}} = \frac{\varepsilon_{\lambda_1,\theta}}{\varepsilon_{\lambda_2,\theta}} \cdot \frac{I_{\lambda_1,BB}}{I_{\lambda_2,BB}}$$

$$I_{\lambda,BB}(\lambda,T) = \frac{2\pi hc^2}{\lambda^5 \cdot \left[exp\left(\frac{hc}{\lambda kT}\right) - 1\right]} \cong \frac{2\pi hc^2}{\lambda^5 \cdot \left[exp\left(\frac{hc}{\lambda kT}\right)\right]}, \text{since } exp(hc/\lambda kT) \gg 1$$

.

.

.

$$T = \frac{hc}{k} \cdot \frac{\left(\frac{1}{\lambda_2} - \frac{1}{\lambda_1}\right)}{\left[ln\left(\frac{\varepsilon_{\lambda_2,\theta}}{\varepsilon_{\lambda_1,\theta}}\right) + ln\left(\frac{I_{\lambda_1,surf}}{I_{\lambda_2,surf}}\right) + ln\left(\frac{{\lambda_1}^5}{{\lambda_2}^5}\right)\right]}$$

Calibration of the ratio of emission intensities to temperature removes emissivity as a variable

- Two-color camera measures temperature based on the ratio of integrated IR emission in two IR regions, not single band intensity

- Mathematically
  - Planck's law for photon emittance [ph/s/cm^2/μm]
  - Radiant emittance from source some fraction of that from a blackbody source [W/cm^2/μm]

- If emissivity, ε, in both wavelengths regions is equal, first term in denominator falls out

$$Q_{BB}(\lambda, T) = \frac{2\pi c}{\lambda^4 \cdot \left[exp\left(\frac{hc}{\lambda kT}\right) - 1\right]} \qquad W(\lambda, T) = \frac{hc}{\lambda} Q(\lambda, T)$$

$$I_{\lambda,surf}(\lambda, \theta, \phi, T) = \varepsilon_{\lambda,\theta}(\lambda, \theta, \phi, T) \cdot I_{\lambda,BB}(\lambda, T)$$

$$\frac{I_{\lambda_1,surf}}{I_{\lambda_2,surf}} = \frac{\varepsilon_{\lambda_1,\theta}}{\varepsilon_{\lambda_2,\theta}} \cdot \frac{I_{\lambda_1,BB}}{I_{\lambda_2,BB}}$$

$$I_{\lambda,BB}(\lambda, T) = \frac{2\pi hc^2}{\lambda^5 \cdot \left[exp\left(\frac{hc}{\lambda kT}\right) - 1\right]} \cong \frac{2\pi hc^2}{\lambda^5 \cdot \left[exp\left(\frac{hc}{\lambda kT}\right)\right]}, \text{since } exp(hc/\lambda kT) \gg 1$$

.

.

.

$$T = \frac{hc}{k} \cdot \frac{\left(\frac{1}{\lambda_2} - \frac{1}{\lambda_1}\right)}{\left[ln\left(\frac{\varepsilon_{\lambda_2,\theta}}{\varepsilon_{\lambda_1,\theta}}\right) + ln\left(\frac{I_{\lambda_1,surf}}{I_{\lambda_2,surf}}\right) + ln\left(\frac{{\lambda_1}^5}{{\lambda_2}^5}\right)\right]}$$

0

NSTX operates with a first-of-its-kind optical dual-band-capable fast IR camera

- Pioneering adaptor based on new commercial IR optical capabilities
- An optical splitter is inserted between the IR camera and lens
  - Contains an IR-specific custom dichroic beamsplitter
  - Diffractive optical element (DOE) hybrid singlet lenses for low chromatic aberration
  - Projects separate IR wavelengths side-by-side on the camera's detector

Dual-band IR adaptor layout

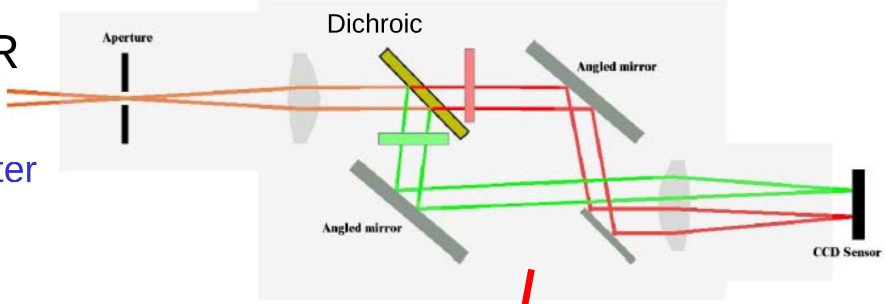

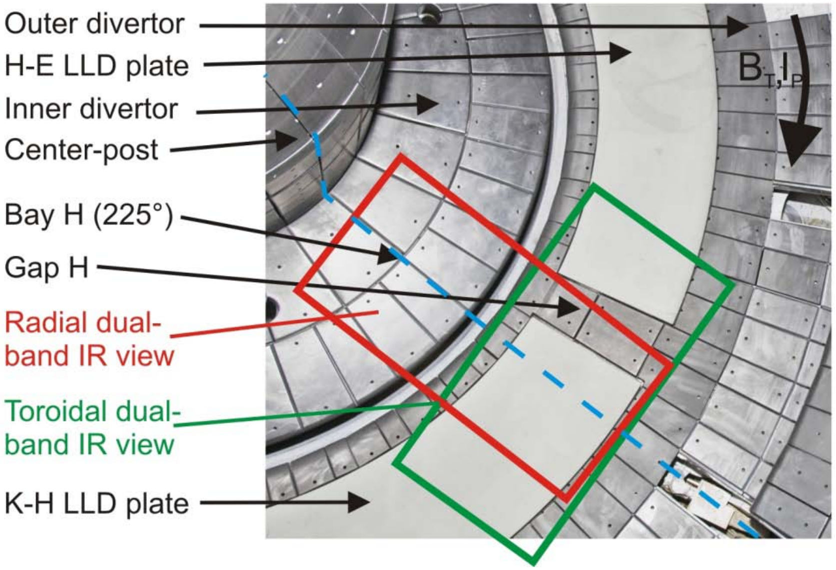

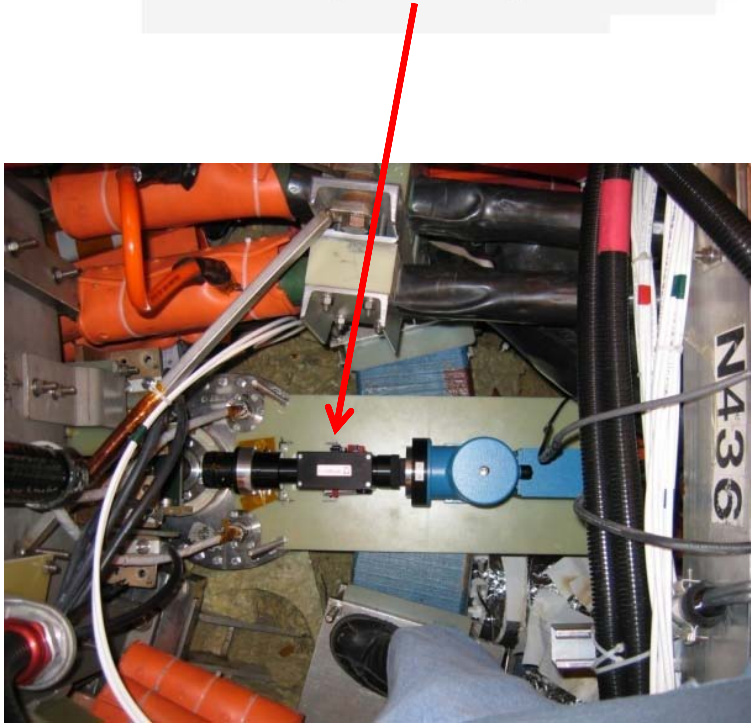

NSTX operates with a first-of-its-kind optical dual-band-capable fast IR camera

- Pioneering adaptor based on new commercial IR optical capabilities
- An optical splitter is inserted between the IR camera and lens
  - Contains an IR-specific custom dichroic beamsplitter
  - Diffractive optical element (DOE) hybrid singlet lenses for low chromatic aberration
  - Projects separate IR wavelengths side-by-side on the camera's detector
- Intensity ratio calibrated vs. temperature *ex-situ* using a blackbody source, and *in-situ* by artificially heating the LLD

Dual-band IR adaptor layout

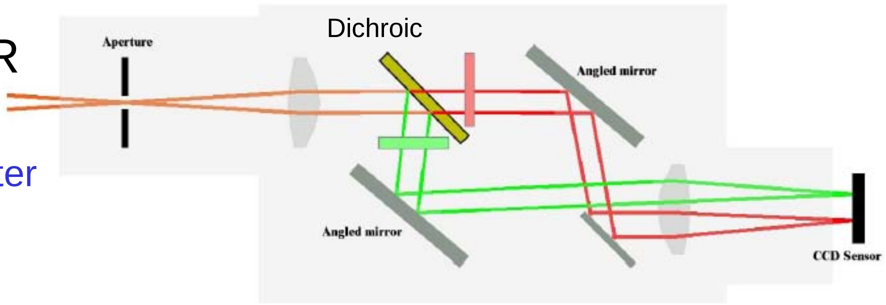

Dual-band intensity ratio calibration

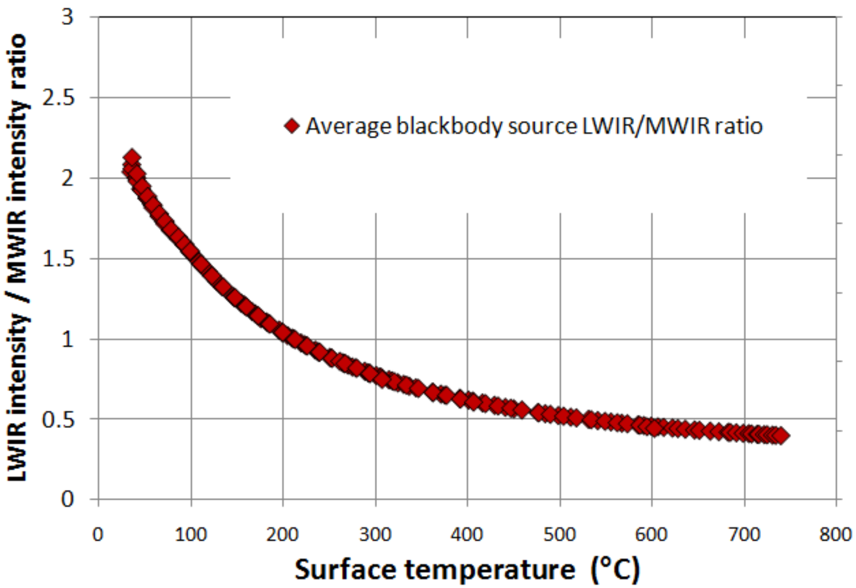

NSTX operates with a first-of-its-kind optical dual-band-capable fast IR camera

- Pioneering adaptor based on new commercial IR optical capabilities
- An optical splitter is inserted between the IR camera and lens
  - Contains an IR-specific custom dichroic beamsplitter
  - Diffractive optical element (DOE) hybrid singlet lenses for low chromatic aberration
  - Projects separate IR wavelengths side-by-side on the camera's detector
- Intensity ratio calibrated vs. temperature *ex-situ* using a blackbody source, and *in-situ* by artificially heating the LLD

Dual-band IR adaptor layout

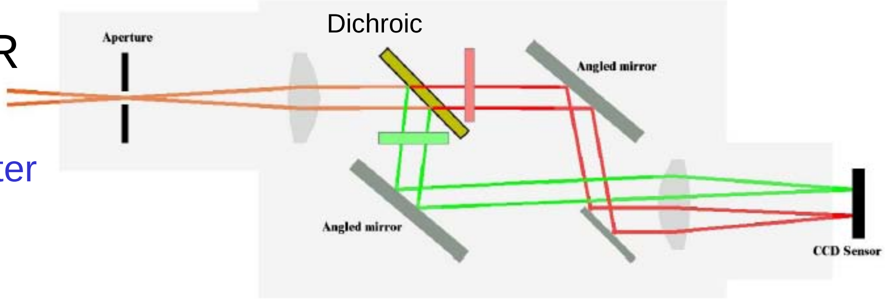

Dual-band intensity ratio calibration

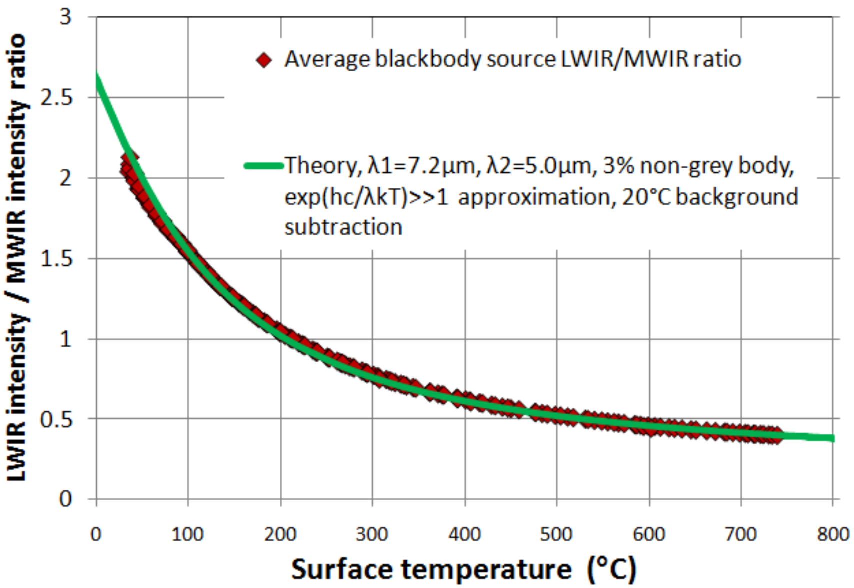

NSTX operates with a first-of-its-kind optical dual-band-capable fast IR camera

- Pioneering adaptor based on new commercial IR optical capabilities
- An optical splitter is inserted between the IR camera and lens
  - Contains an IR-specific custom dichroic beamsplitter
  - Diffractive optical element (DOE) hybrid singlet lenses for low chromatic aberration
  - Projects separate IR wavelengths side-by-side on the camera's detector
- Intensity ratio calibrated vs. temperature *ex-situ* using a blackbody source, and *in-situ* by artificially heating the LLD
- Dual-band IR cameras now available from three companies worldwide
  - Integrate two detecting elements into each pixel
  - However, all limited to ≤300 Hz frame rate
  - $200+k cost, 3-6 month lead time
- Optical image splitter: $20k total cost, adaptable to any IR camera

Dual-band IR adaptor layout

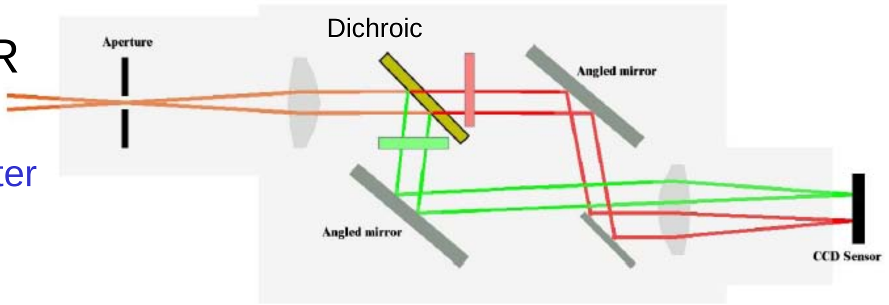

Dual-band intensity ratio calibration

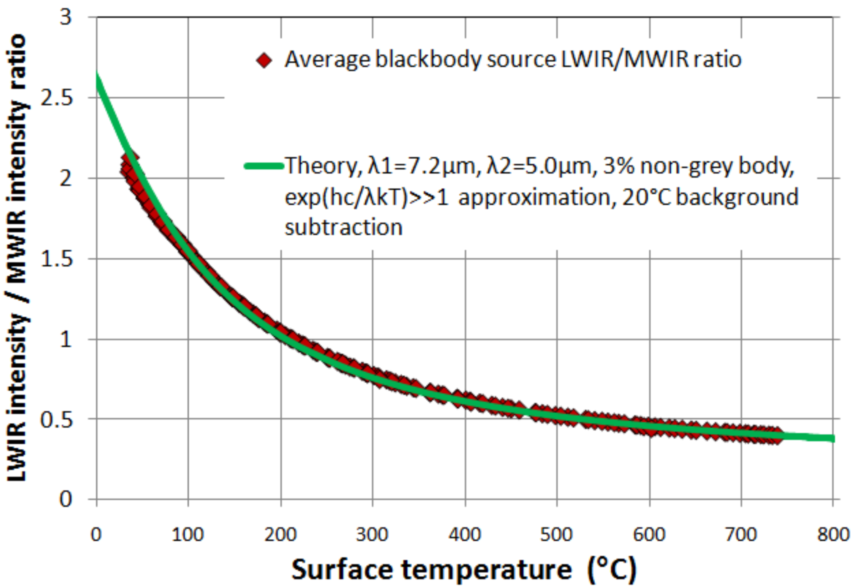

Interpretation of NSTX data viewing the LLD in single-band intensity vs. dual-band ratio demonstrates the technique

- Independent calibrations in both single-bands (MWIR and LWIR), and calibration using the **dual-band ratio** are performed

Surface temperature measured by the fast IR camera at the outer strike point in an NSTX plasma discharge

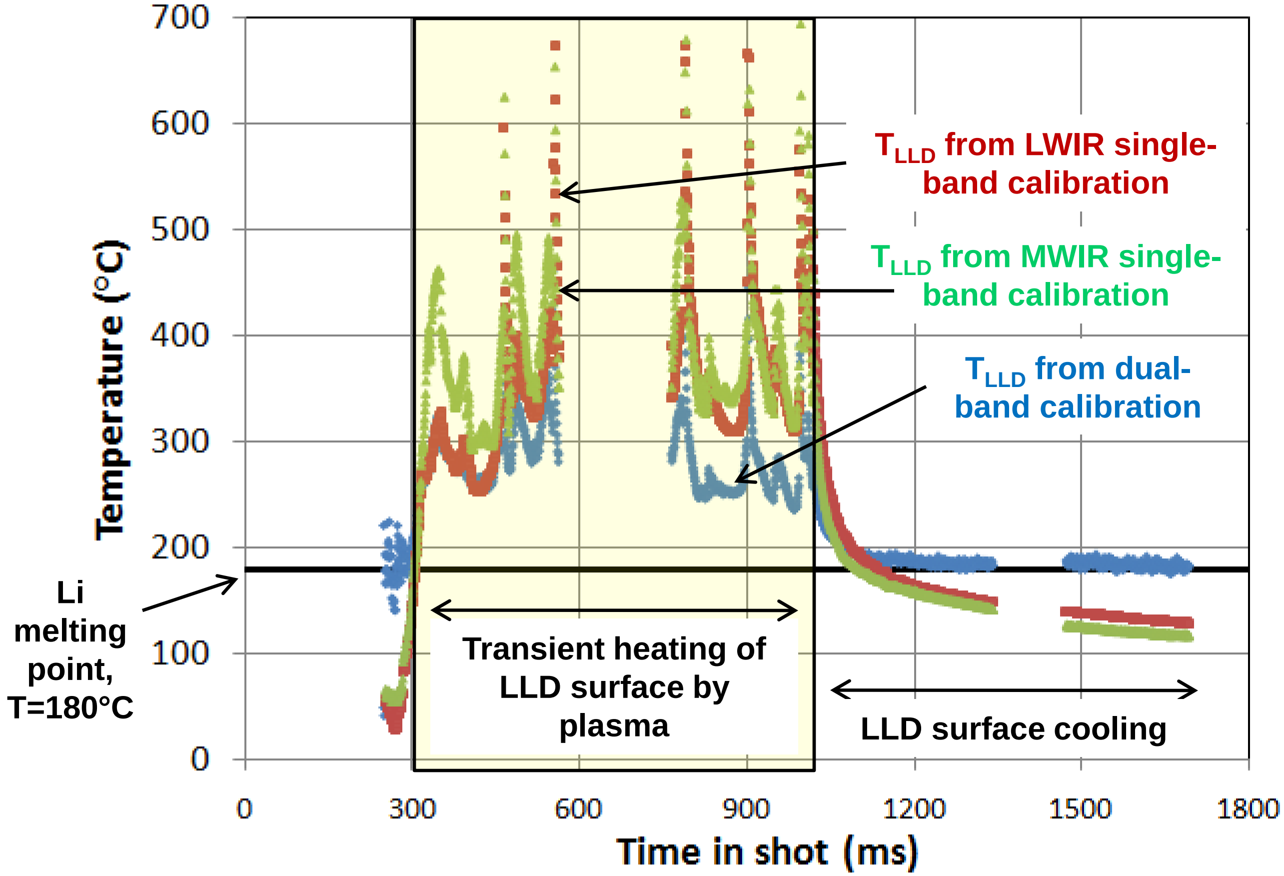

Interpretation of data in single-band intensity vs. the dual-band ratio demonstrates that the technique works

- Independent calibrations in both single-bands (MWIR and LWIR), and calibration using the **dual-band ratio** are performed
- In single-band results, apparent LLD surface temperature reduces monotonically after ~1000 ms
  - Change in emissivity as Li solidifies not accounted for
- **However, dual-band calibrated temperature steadies at Li melting temperature**
  - Indicator of latent heat of solidification
- Bonus: Ratio between single-band and dual-band temperature is a measure of surface emissivity

Surface temperature measured by the fast IR camera at the outer strike point in an NSTX plasma discharge

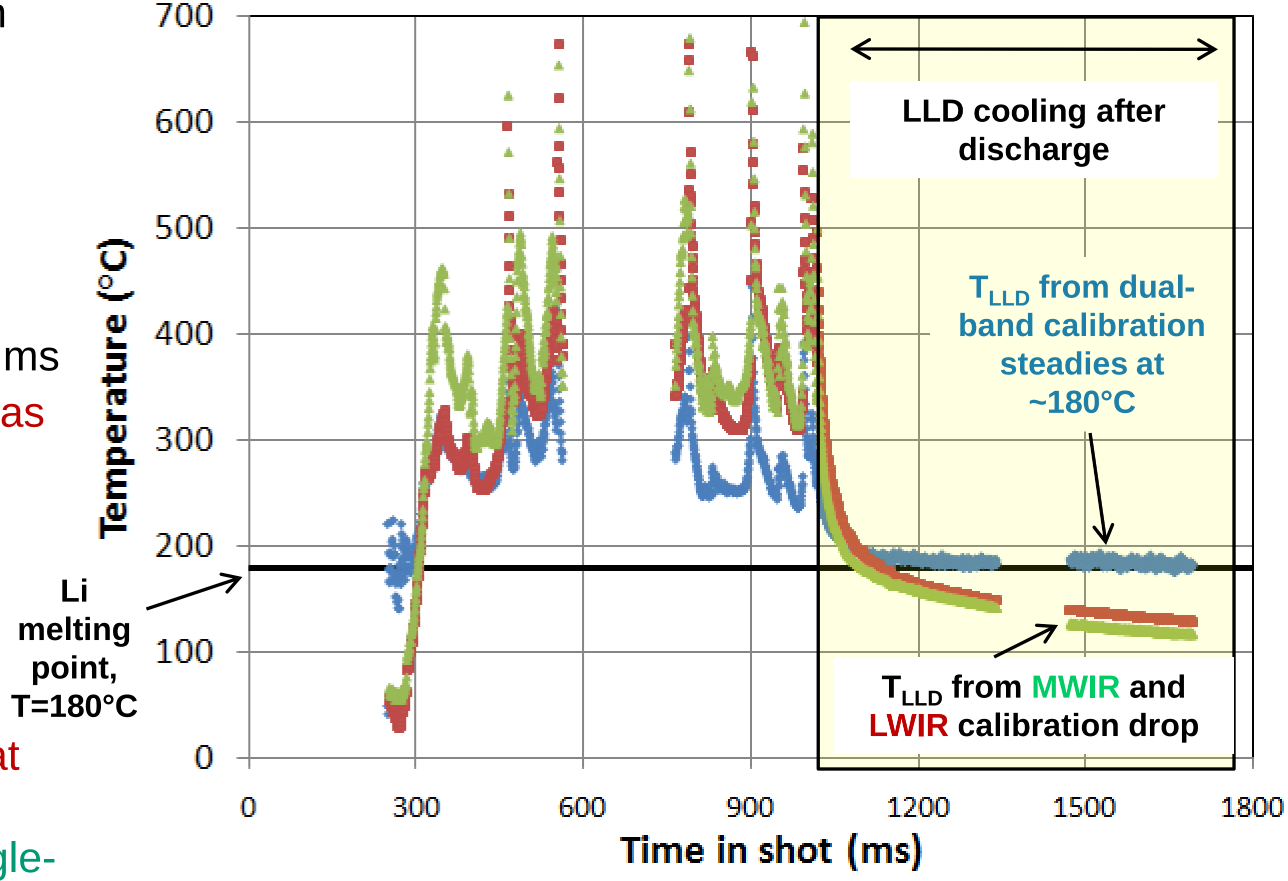

**** All subsequent data shown is dual-band***

Outline

- Dual-band infrared technique demonstrated in NSTX in 2010
- Li melt dynamics on the LLD
- LLD vs. graphite tile surface temperature: Observation of clamping
- Edge plasma modification with and without Li deposition
- Conclusions

Incremental plasma exposure in discharge series on the LLD causes the melted area to increase

- Heating of the LLD surface over a series of repeat discharges demonstrates how the Li surface is heated
  - ~30% of total LLD surface at > Li melting at beginning of series
  - Melted fraction does not change significantly in one discharge

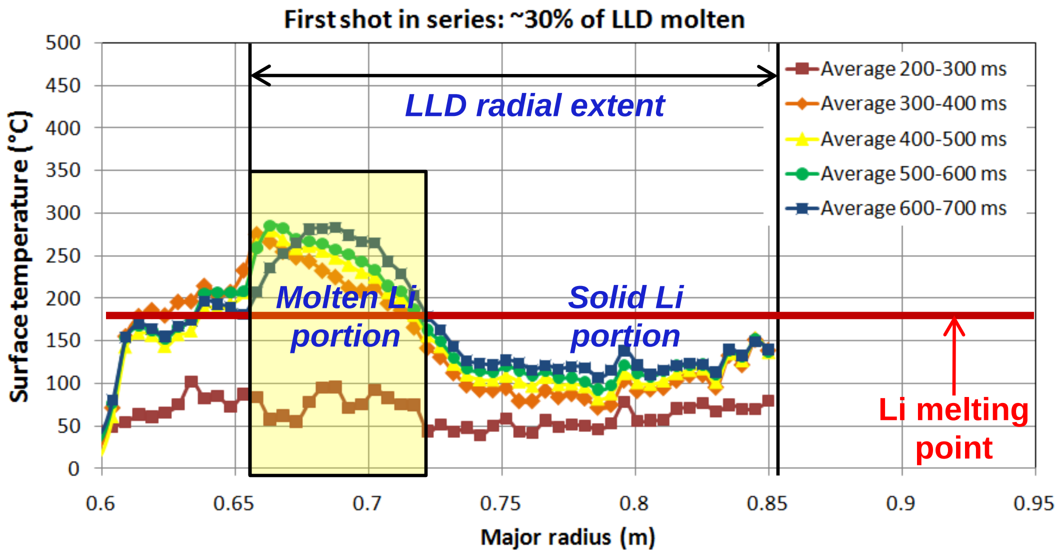

Incremental plasma exposure in discharge series on the LLD causes the melted area to increase

- Heating of the LLD surface over a series of repeat discharges demonstrates how the Li surface is heated
  - ~30% of total LLD surface at > Li melting at beginning of series
  - Melted fraction does not change significantly in one discharge
- Melted area increases to ~90% of LLD surface by end of discharge series

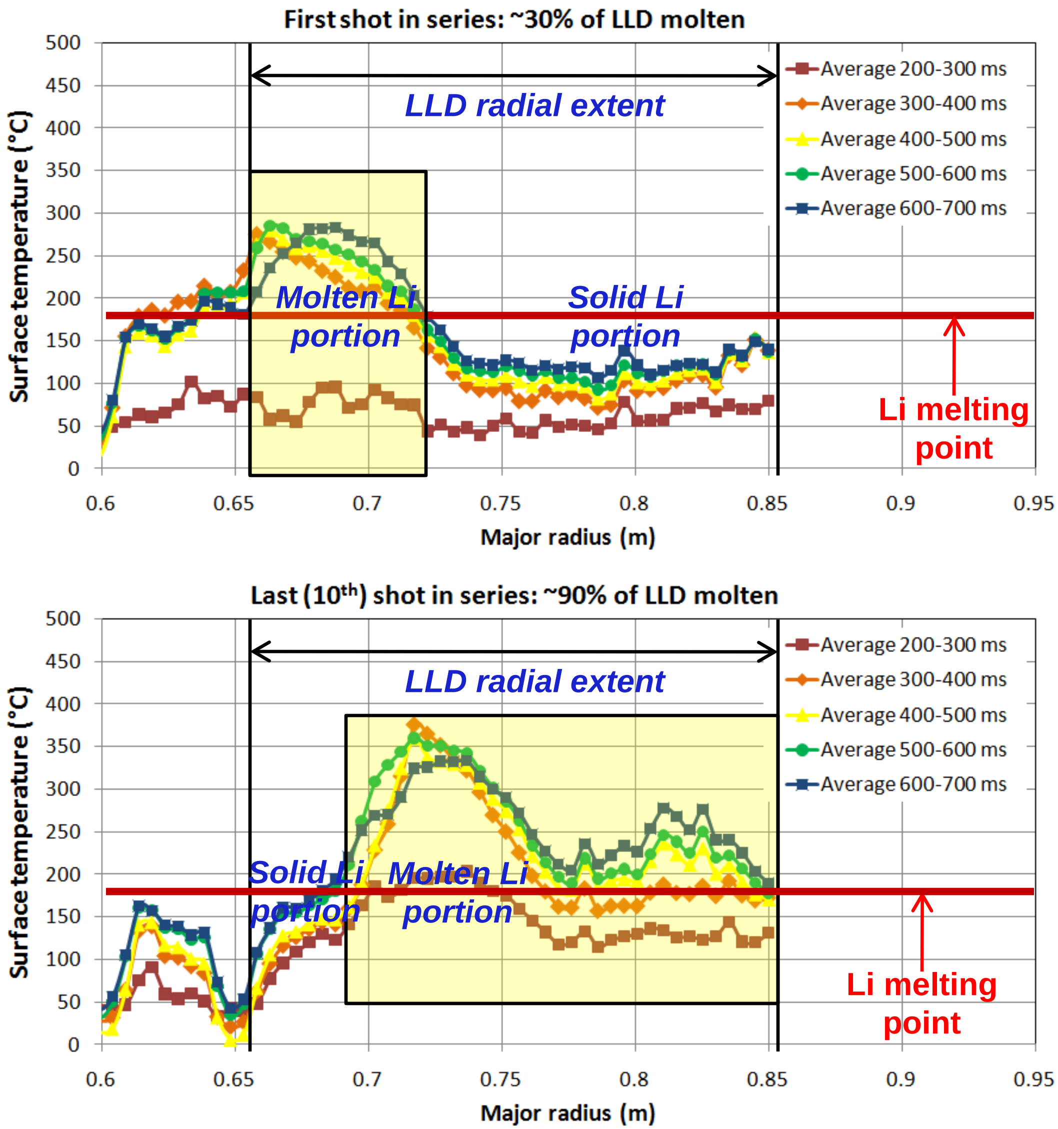

Transient power excursions (ELMs) on the LLD cause brief heating of surface to >500°C

- ELMs can occur frequently on the LLD, depending on plasma geometry and conditions
- Temperature during ELMs briefly (<5 ms) reach >400°C
- Further study required to determine whether this may be a significant Li evaporation loss mechanism

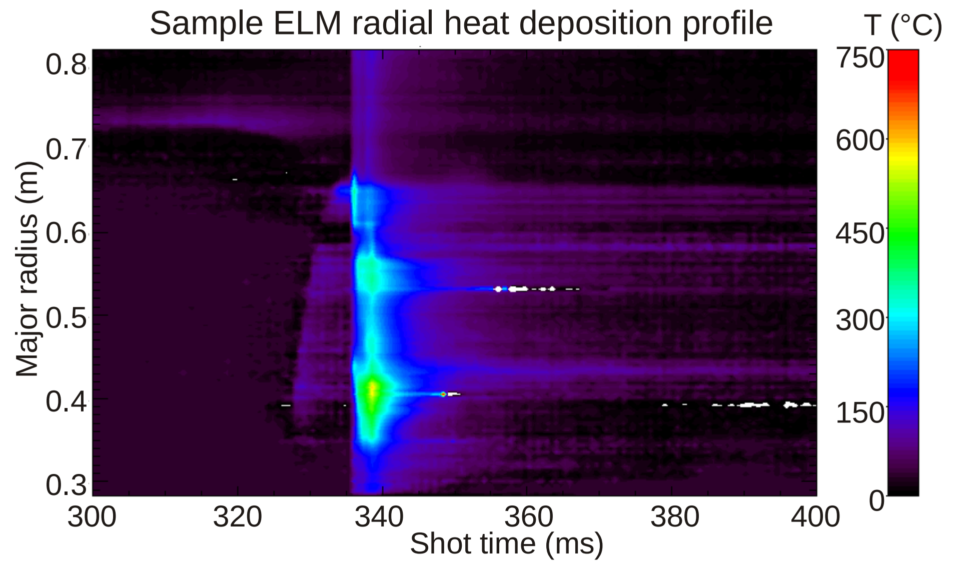

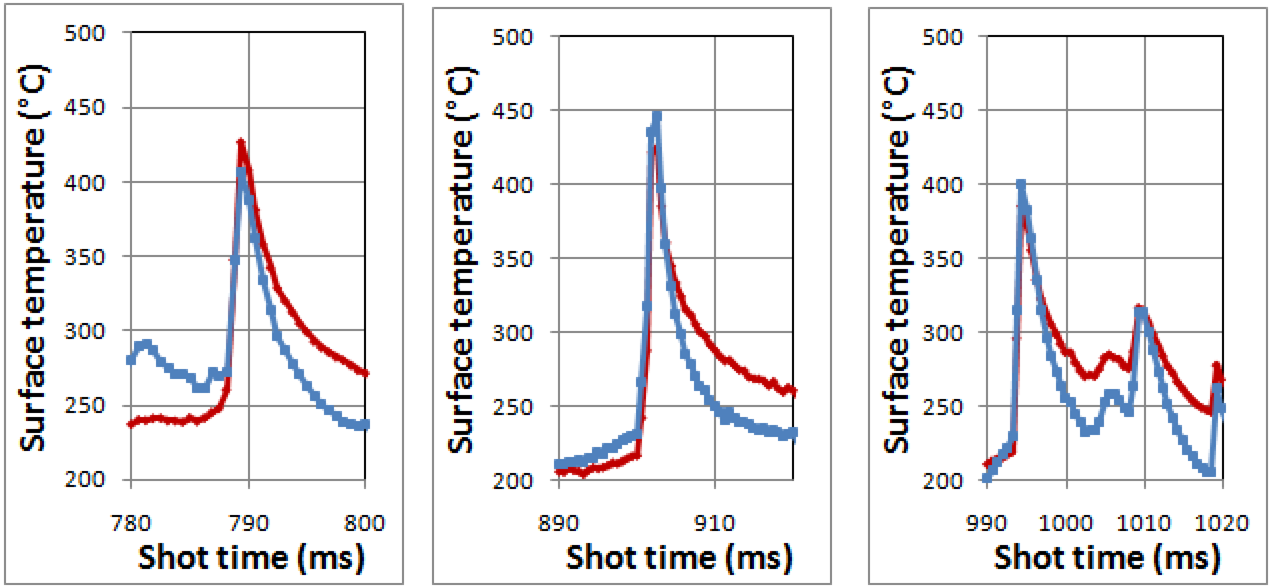

Outline

- Dual-band infrared technique demonstrated in NSTX in 2010
- Li melt dynamics on the LLD
- LLD vs. graphite tile surface temperature: Observation of clamping
- Edge plasma modification with and without Li deposition
- Conclusions

T_{avg} near OSP on LLD and graphite tile at equal radii suggests that Li in the LLD is causing clamping of the temperature

- Series of 10 repeat discharges with outer strike point on the LLD
- Graphite and LLD in this case begins with T_{Li}~70°C
- T_{avg} on graphite gap tile increases through all shots in SQRT(t) fashion

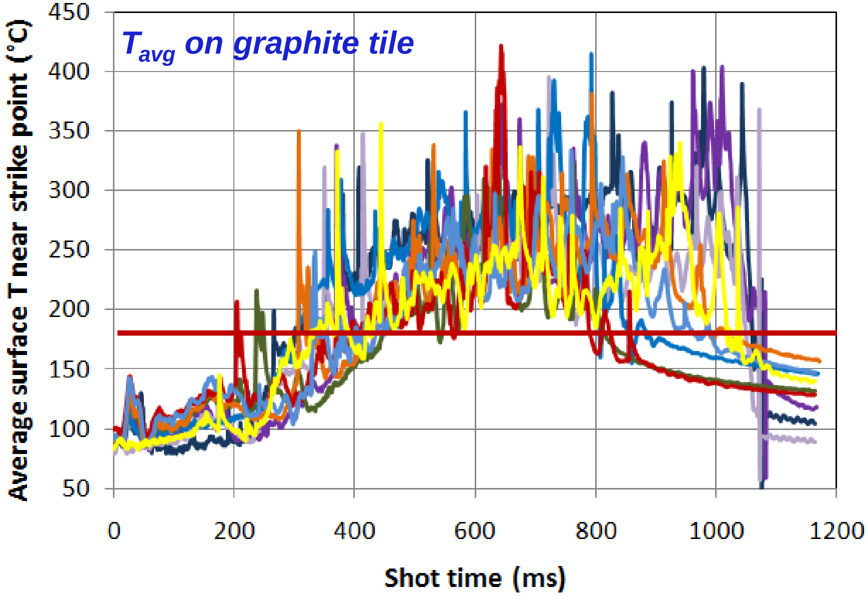

T_{avg} near OSP on LLD and graphite tile at equal radii suggests that Li in the LLD is causing clamping of the temperature

- Series of 10 repeat discharges with outer strike point on the LLD
- Graphite and LLD in this case begins with T_{Li}~70°C
- T_{avg} on graphite gap tile increases through all shots in SQRT(t) fashion
  - Average $T_{surface}$ of ~250°C
- Falls back to ambient post-discharge

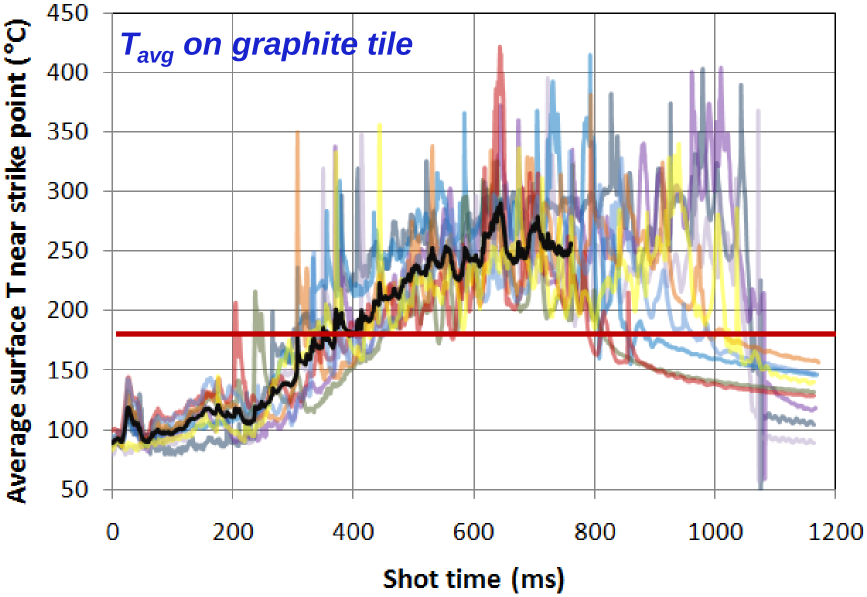

T_{avg} near OSP on LLD and graphite tile at equal radii suggests that Li in the LLD is causing clamping of the temperature

- Series of 10 repeat discharges with outer strike point on the LLD
- Graphite and LLD in this case begins with T_{Li}~70°C
- T_{avg} on graphite gap tile increases through all shots in SQRT(t) fashion
    - Average $T_{surface}$ of ~250°C
- Falls back to ambient post-discharge
- T_{avg} plotted at same radius, but on LLD

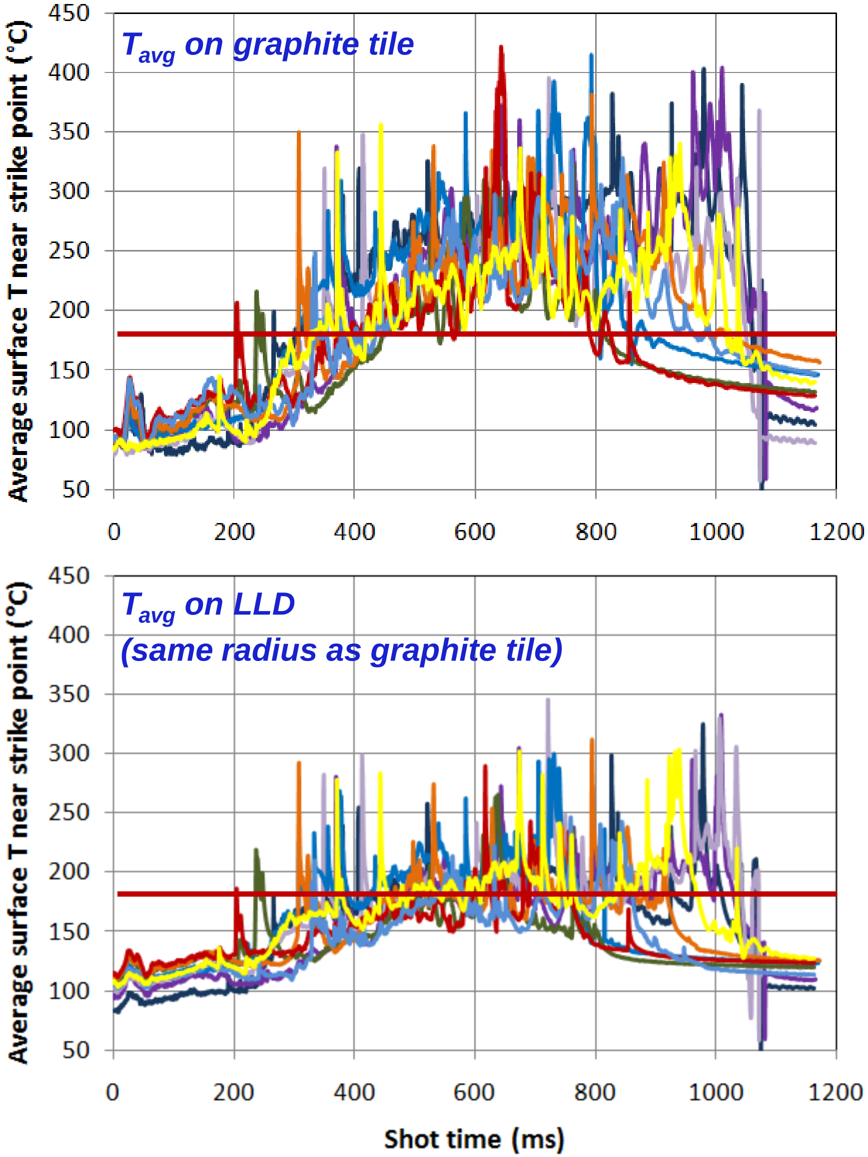

T_{avg} near OSP on LLD and graphite tile at equal radii suggests that Li in the LLD is causing clamping of the temperature

- Series of 10 repeat discharges with outer strike point on the LLD
- Graphite and LLD in this case begins with T_{Li}~70°C
- T_{avg} on graphite gap tile increases through all shots in SQRT(t) fashion
    - Average $T_{surface}$ of ~250°C
- Falls back to ambient post-discharge
- T_{avg} plotted at same radius, but on LLD
- T_{avg} on LLD surface gravitates at $T_{melt,Li}$ (average $T_{surface}$ of ~180°C) throughout discharges, increases with ELMs
    - Efficient heat removal in liquid Li?
    - Li radiation?
    - Vapor shielding playing a role?

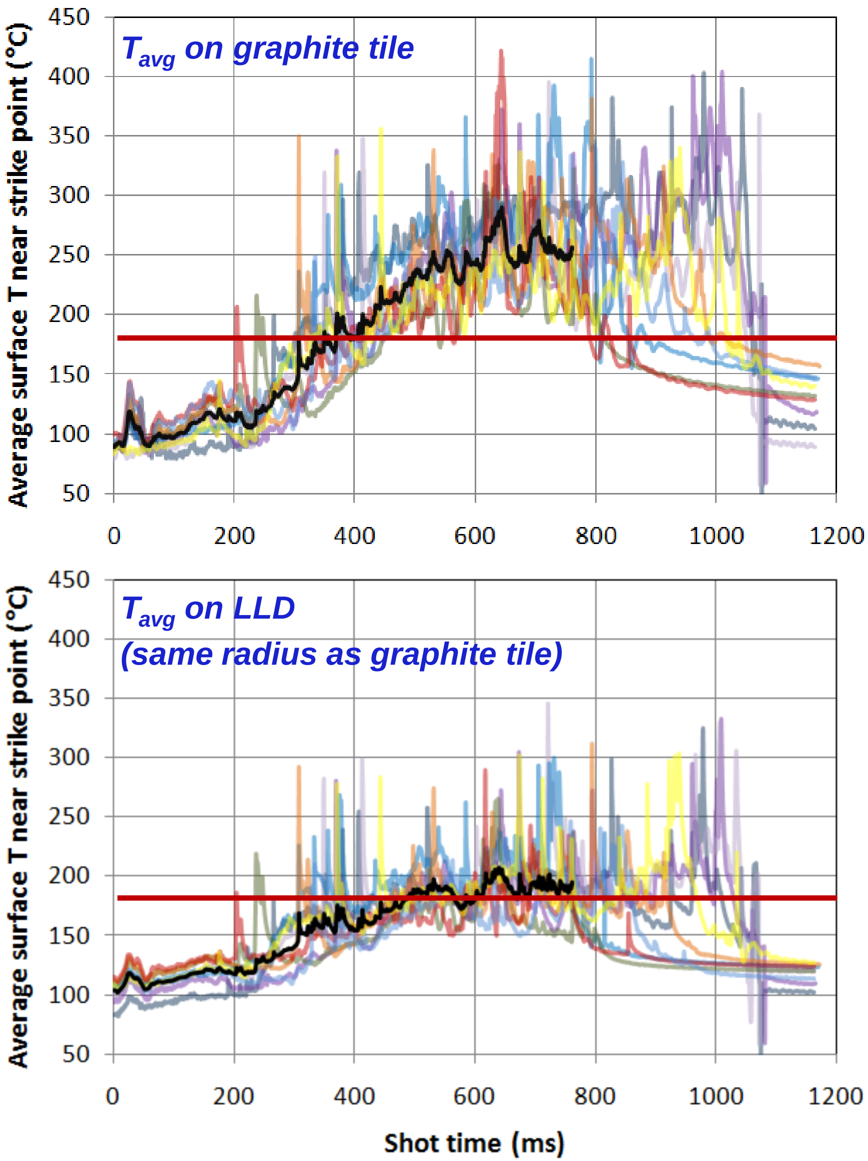

T_{avg} near OSP on LLD and graphite tile at equal radii suggests that Li in the LLD is causing clamping of the temperature

- Series of 10 repeat discharges with outer strike point on the LLD
- Graphite and LLD in this case begins with T_{Li}~70°C
- T_{avg} on graphite gap tile increases through all shots in SQRT(t) fashion
  - Average $T_{surface}$ of ~250°C
- Falls back to ambient post-discharge
- T_{avg} plotted at same radius, but on LLD
- T_{avg} on LLD surface gravitates at $T_{melt,Li}$ (average $T_{surface}$ of ~180°C) throughout discharges, increases with ELMs
  - Efficient heat removal in liquid Li?
  - Li radiation?
  - Vapor shielding playing a role?
- Insufficient energy to maintain Li 'bulk' at Li melting temperature
  - Measured response dominated by thin upper surface

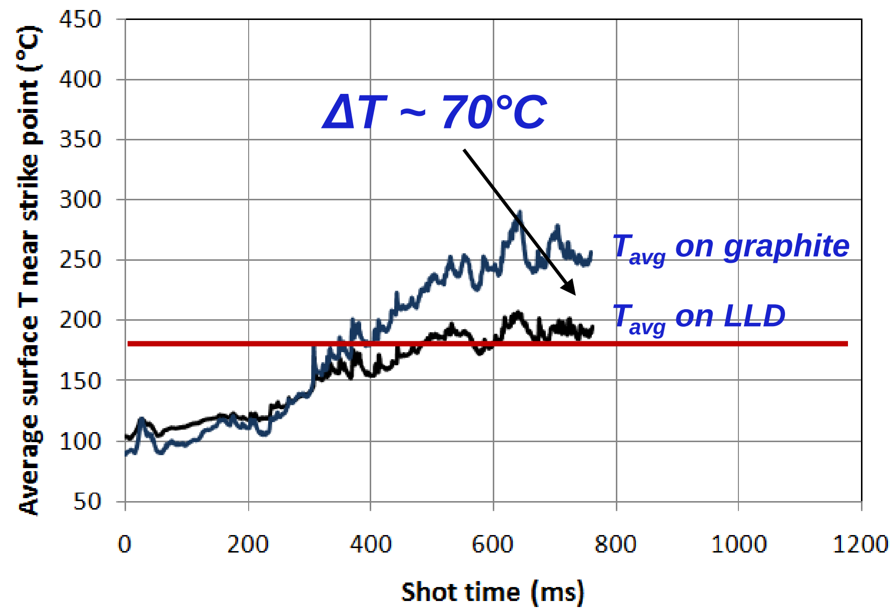

Outline

- Dual-band infrared technique demonstrated in NSTX in 2010
- Li melt dynamics on the LLD
- LLD vs. graphite tile surface temperature: Observation of clamping
- Edge plasma modification with and without Li deposition
- Conclusions

The IDL-based FURNACE analysis suite integrates dual-band IR calibration and analysis for NSTX database

- Semi-automated image alignment, (spatial/temporal/temperature) calibration, and heat flux calculation for any shot in the 2010 NSTX database
  - Ratio profile highly dependent on accurate band image alignment
- Incorporation of 1-D Carslaw & Jaeger heat flux calculation and THEODOR (A. Herrmann) for determination of 2-D heat flux (q)
  - Adds thin layer with poor thermal contact, artificially high heat transmission coefficient, α
  - Value of α estimated based on power balance through the shot
- 1-D vs. radius, 1-D vs. time, 2-D output for ease of visualization

Raw dual-band data

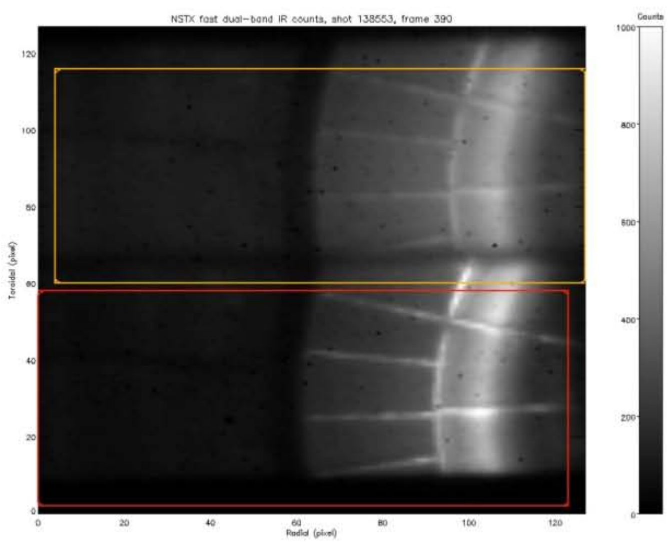

Aligned, calibrated

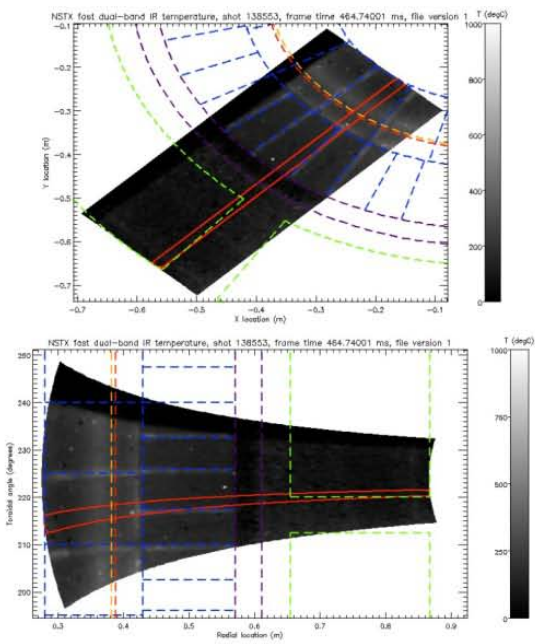

T(R,t), q(R,t)

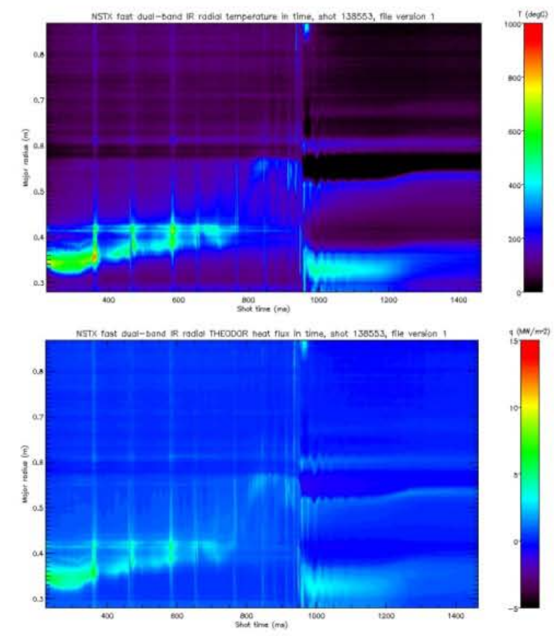

Divertor λ_q contracts with increasing lithium deposition

- Type V ELMs eliminated from discharges with Li deposition
  - Some sporadic type I ELMs are still present
  - Responsible for some of the contraction in IR profiles
- λ_q^{div} contracts further with increasing lithium deposition
- This effect is confirmed by dual-band IR measurements

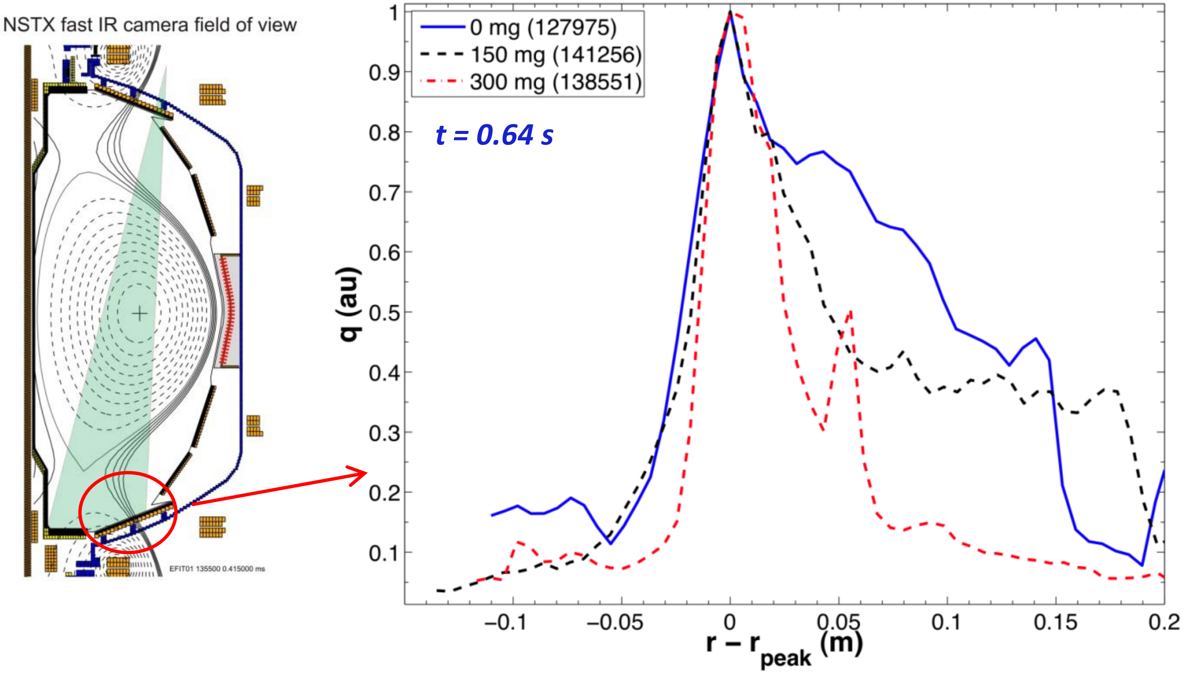

	0 mg	150 mg	300 mg
λ_q^{div} (cm)	14.1	13	7
λ_q^{mid} (cm)	0.98	0.74	0.37

Outline

- Dual-band infrared technique demonstrated in NSTX in 2010
- Li melt dynamics on the LLD
- LLD vs. graphite tile surface temperature: Observation of clamping
- Edge plasma modification with and without Li deposition
- Conclusions

LLD temperature dynamics provide a glimpse of an operating regime for Li as a Tokamak first-wall material

- Dual-band IR measurement of LLD surface proven effective
- Front face thermal properties of the LLD are dominated by the Cu substrate → See the poster on Friday
- Surface temperature dynamics heavily dependent on total surface area with $T > T_{melt,Li}$
- LLD surface shows significant signs of clamping in peak and radially averaged temperature compared to graphite where no clamping occurs
- Deposition of increasing amounts of Li leads to contraction of the heat flux profile → Adds to challenge

Outline

- Dual-band infrared technique demonstrated in NSTX in 2010
- Li melt dynamics on the LLD
- LLD vs. graphite tile surface temperature: Observation of clamping
- Edge plasma modification with and without Li deposition
- Conclusions
- *Time permitting: Thermal diagnostic improvements on NSTX for 2011*

Wide-angle two-color IR camera on NSTX

J. Nichols, A. McLean, J. Ahn, K. Gan, R. Maingi, L. Roquemore, B. Stratton, T. Gray

- Wide-angle, high-resolution temperature and heat flux measurements
  - Dynamic range similar to existing dual-band camera
  - Straightforward observation of non-axisymmetric phenomenon
- Two color: 8-10 µm and 10.5-13 µm in the LWIR band
  - FLIR Tau 640x480, 30 Hz, LWIR microbolometer camera
- Radial/toroidal configurations
  - Diagnosis of Moly tiles
  - High-res radial profile out to R=120 cm
  - 180° coverage of OSP
  - 4 mm spatial resolution
- Optical relay to locate camera outside of magnetic field
  - Re-entrant tube with CVD diamond window
    - Allows 450°C bake uncooled
  - Reflective ellipsoidal light collection (based on ITER/JET design)
  - BBAR coated ZnSe optics, Au-coating reflective surfaces

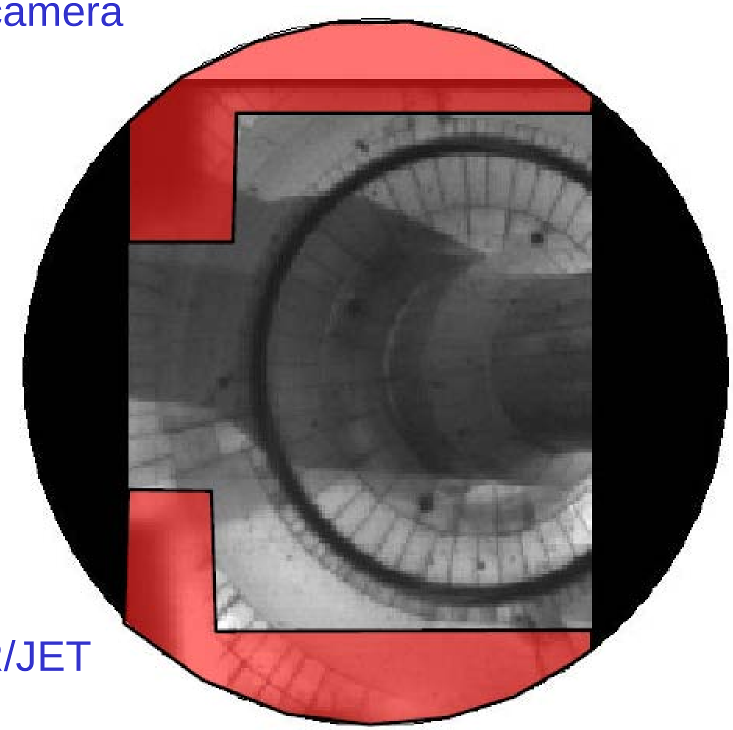

Fast 'eroding' thermocouples (TCs) for NSTX

A. McLean, J. Ahn, T. Gray, H. Kugel, R. Maingi, L. Roquemore

- Standard TC junctions have ~100 ms response time due to thermal mass
  - Existing array of TCs in NSTX not active during plasma discharges
- Junction in 'eroding' or 'self-renewing' thermocouples forms dynamically between ribbons (0.0015" thick) separated by thin (0.0002") dielectric insulator layers
  - Used in transient high heat-flux environments (rockets, gun barrels, recently on C-Mod)
  - ~1 ms response time, in direct plasma contact to provide direct benchmark of heat flux measured by infrared cameras
- Strong collaboration with patent holder, Nanmac (Ma. US, www.nanmac.com)
- High temperature Type C design
  - Tungsten (W) / Rhenium (Re), 0-2320°C range

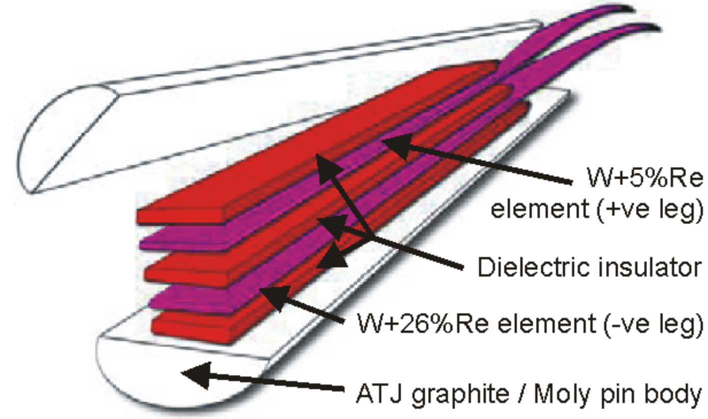

Tile #1 underside

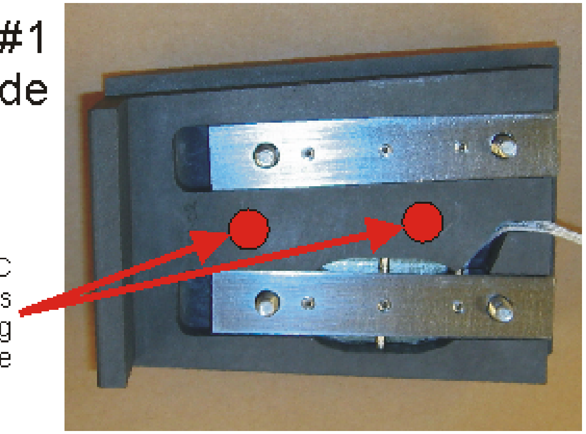

Poloidal cross section

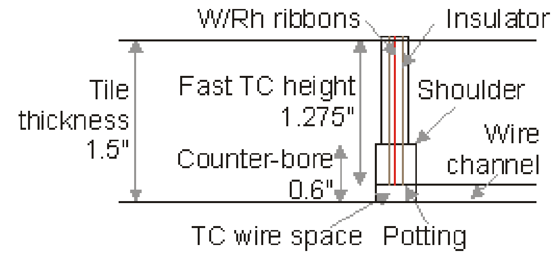

Two fast thermocouple have been installed for use in 2011

- Initially, single pair of self-renewing TCs with graphite body installed in this vent
  - Units in Gap H tile 1
  - Optimal observation by IR cameras
  - Overlaps radial extent of Langmuir probe array
- Additional pair of Mo-body TCs
  - Installation in Mo tile row next vent
- High temperature twisted Type C wire
  - Omega EXGG-C glass braided (max 427°C)
  - Twisted for low noise, covered with fiberglass sleeving (Markel Thermoflex-1200, max 650°C)
  - Assembly baked to 400°C for 16 hours (Jurczynski)
- High-speed (1 kHz) integrated signal conditioning, cold-junction compensation, plus isolation and self calibration
  - VTI EX1000A series controller (32 channels)
  - Ethernet for post-shot upload to MDSplus

Fast dual-band IR view from Bay H

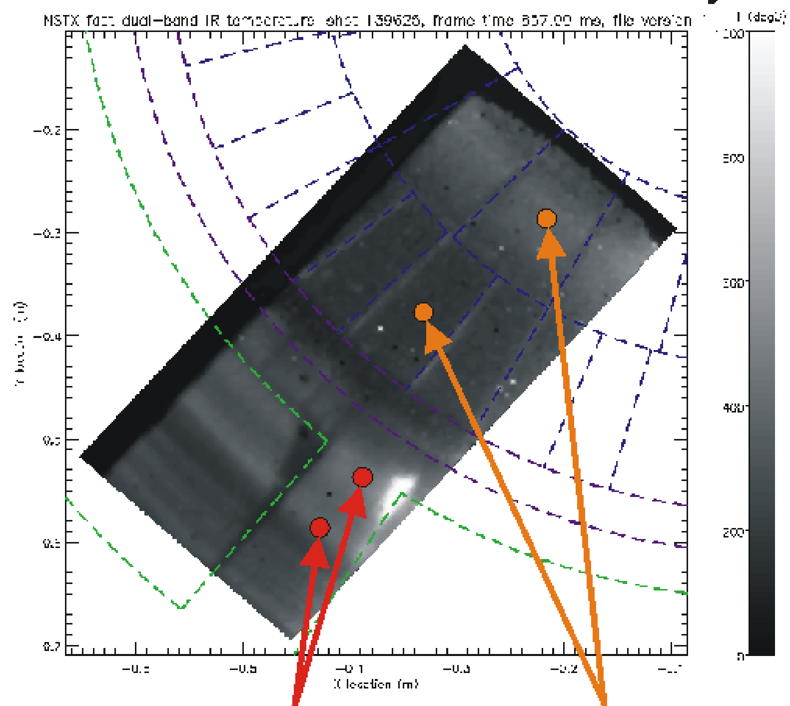

Proposed graphite fast TC locations (2011)

Proposed moly fast TC locations (2012)

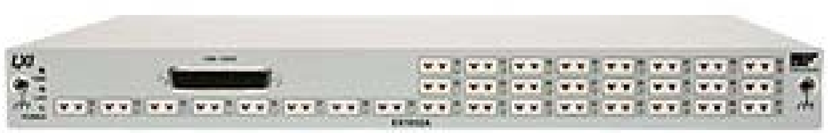

Backup slides

ORNL NSTX Fast Infrared Camera View
Dual-band, radial configuration

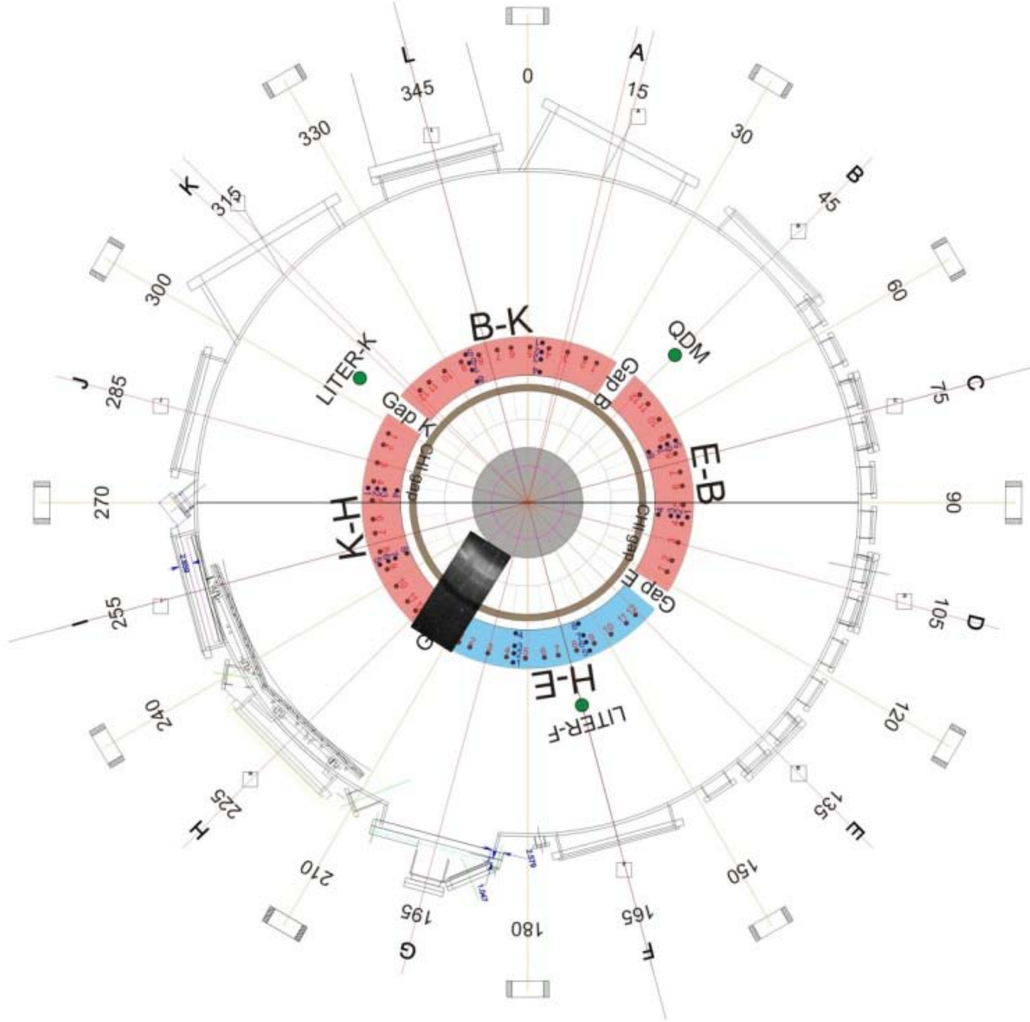

Peak temperature on LLD significantly less than that of Gap H tile

- Peak temperature of LLD at OSP significantly less than that on graphite
- Peak temperature on LLD surface reached prior to that on graphite
- Larger radial fraction of LLD surface reaches Li melting temperature

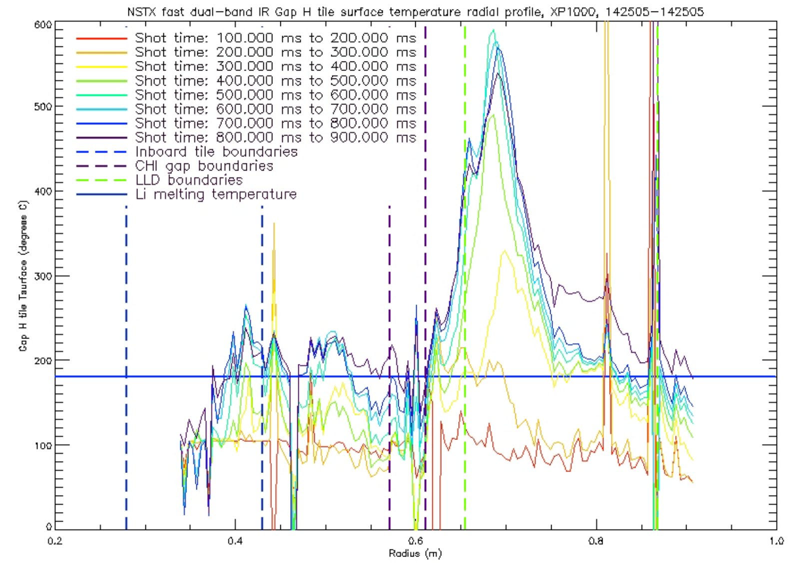

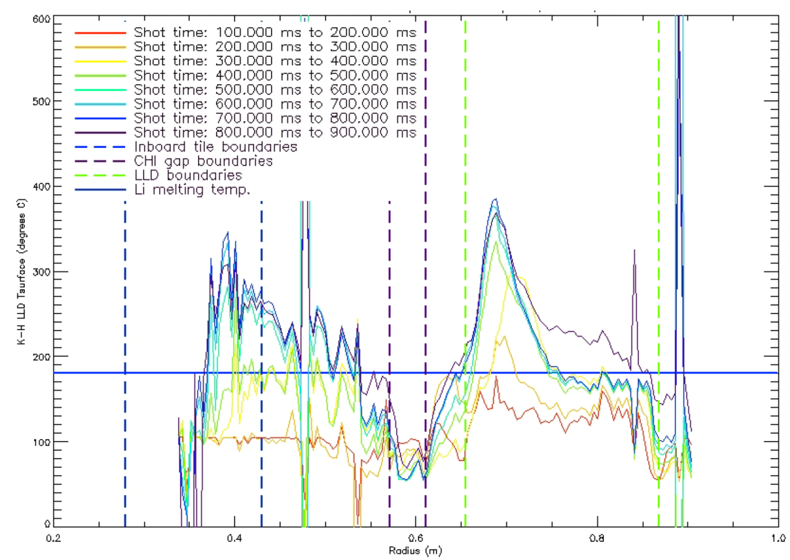

Backup slides

- T_{avg} of LLD surface at equal points in repeat shots as LLD heats up
- Suggests that thermal capacity of Li layer does not substantially change with LLD bulk temperature

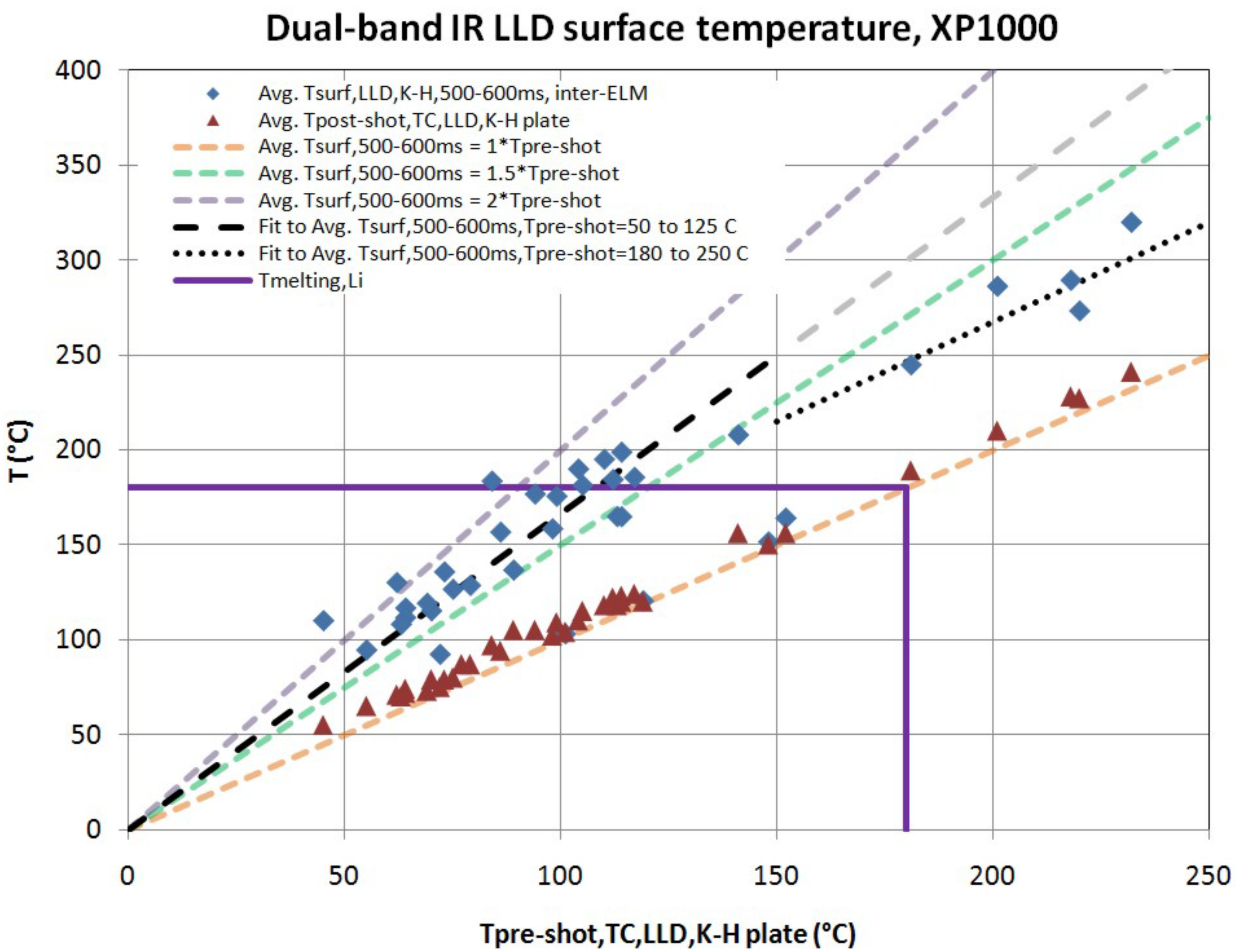

Primary dual-band IR adaptor components

- Long-wave pass dichroic beamsplitter
  - Lambda Research Optics (CA, US)
  - Long-wave pass (7-10 μm transmit with T_{avg}~92%)
  - Medium-wave reflect (4-6 μm reflect with T_{avg}~99%)
- Image splitter optical platform
  - CAIRN Research OptoSplit II (UK)
  - Extensively modified for operation in IR
  - Precision multi-axis optical alignment, focusing, flexibility

- Lenses
  - Broadband AR-coated Diffractive Optical Element (DOE) hybrid singlet lenses
    - 10X reduction in chromatic aberration, reduced spherical aberration, improved SNR compared to meniscus lenses
  - II-VI Infrared (PA, US)
- Shortwave pass (SWP) and longwave pass (LWP) IR filters to limit spectral contamination in each channel
  - Reynard Corporation (CA, US)
- Custom designed lens adaptors/mounts

3D CAD model of fast IR camera and dual-band adapter

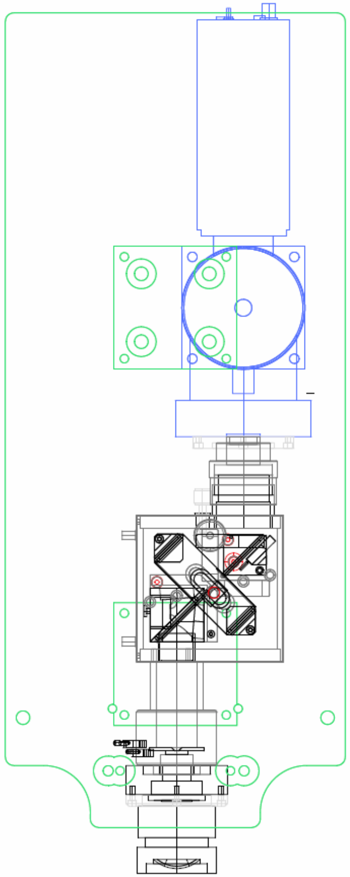

- Dual-band adaptor may be rotated 90° in order to acquire a radial (as pictured) or toroidal view

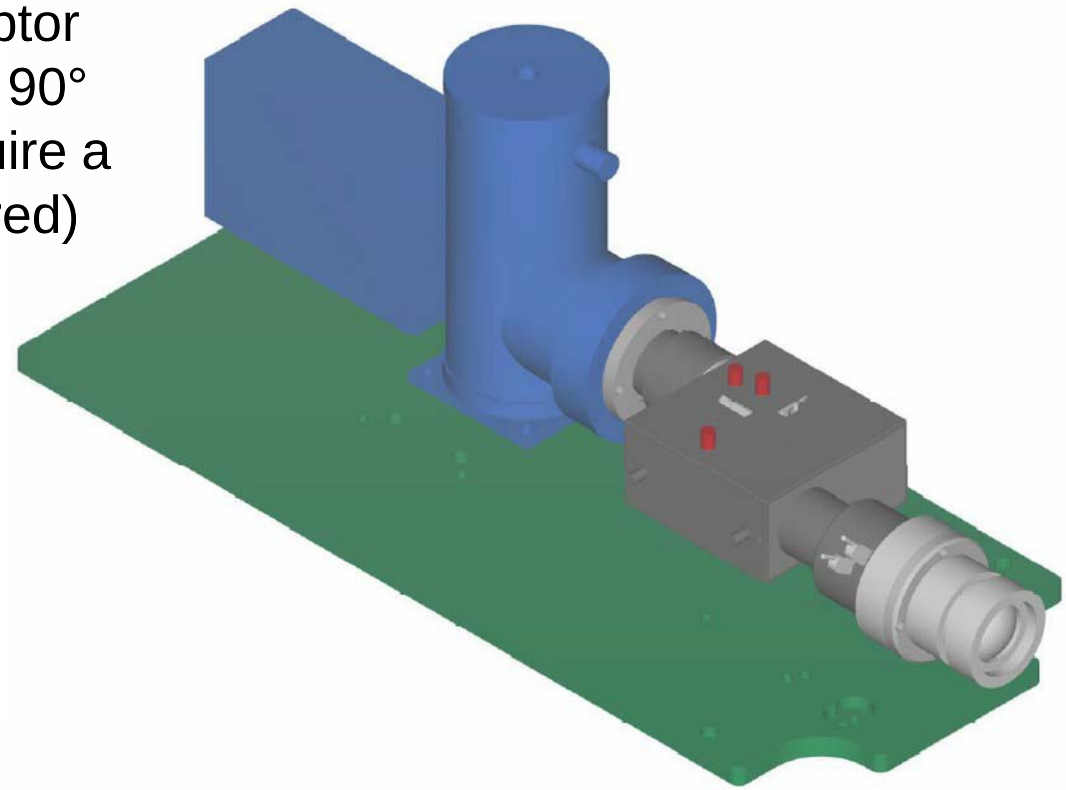

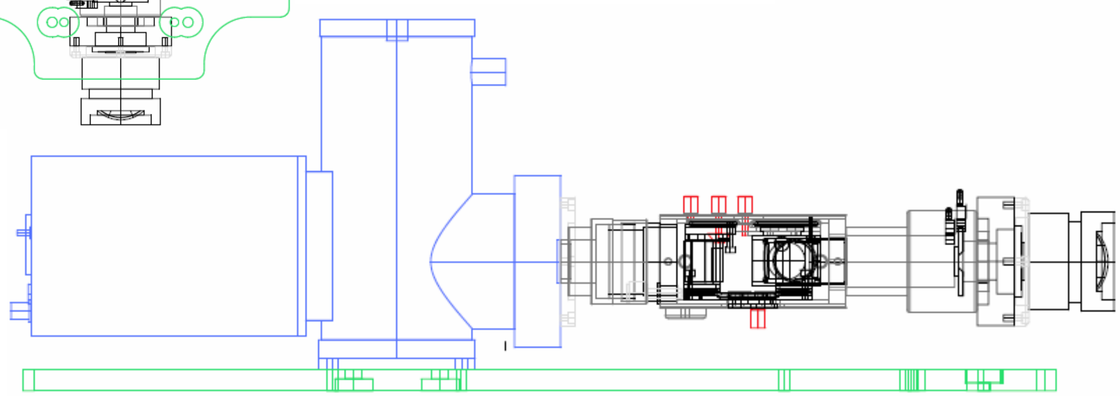

Spectral throughput comparison for IR camera assembly

- Comparison of ideal throughput losses due to optical components in the dual-band adaptor
- Initial dual-band adaptor reduces throughput by ~4X compared to highest efficiency single-band mode
- Near-term improvements will reduce the difference to ~2X
- Significant margin is available in terms of integration time and dynamic range
  - Drop in transmission has no impact on required performance characteristics

Optical element		Wideband operation		Dual-band operation meniscus lenses		Dual-band operation DOE lenses	
		8–12 μm operation	3–12 μm operation	4–6 μm band	7–10 μm band	4–6 μm band	7–10 μm band
Observed bandwidth		4 μm	9 μm	2 μm	3 μm	2 μm	3 μm
Bay H port window		98%	83%	70%	96%	70%	96%
Perp. View mirror		98%					
IR primary lens		95%	75%				
Dual-band adapter	Input lens	N/A		70%	72%	95%	97%
Dual-band adapter	Mirror 1	N/A		98%			
Dual-band adapter	Dichroic	N/A		99%	92%	99%	92%
Dual-band adapter	Short pass filter	N/A		N/A	83%	N/A	83%
Dual-band adapter	Long pass filter	N/A		95%	90%	95%	90%
Dual-band adapter	Mirror 2	N/A		98%			
Dual-band adapter	Output lens	N/A		70%	72%	95%	97%
Camera window		95%	96%	97%	97%	97%	97%
Two-color adapter		N/A		**44%**	**34%**	**82%**	**62%**
Overall transmission		**87%**	**59%**	**22%**	**23%**	**41%**	**43%**

Demonstrated application of dual-band IR with extensive *ex-situ* calibration

- Accomplished with fast camera + dual-band adaptor viewing a blackbody IR source
  - Electro Optical Industries WS162 capable of up to 750°C
  - 400+ frames of data taken with 10-75 μs integration time at 1610 Hz frame rate (1.6-12% duty cycle)
- Useful, low error LWIR/MWIR ratio from ~100-600˚C
  - Altering IR camera system gain will be explored to see if the useful range of the ratio can be extended up to ~1,000˚C

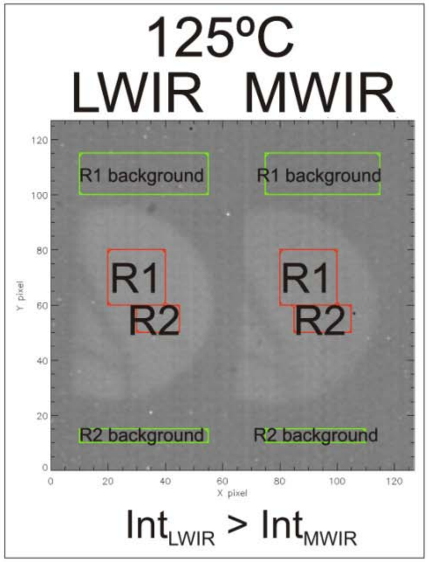

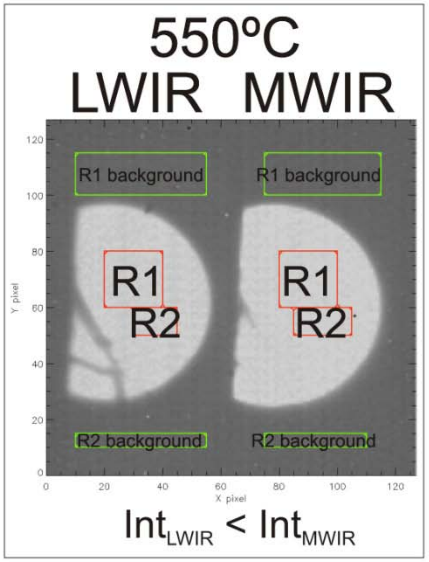

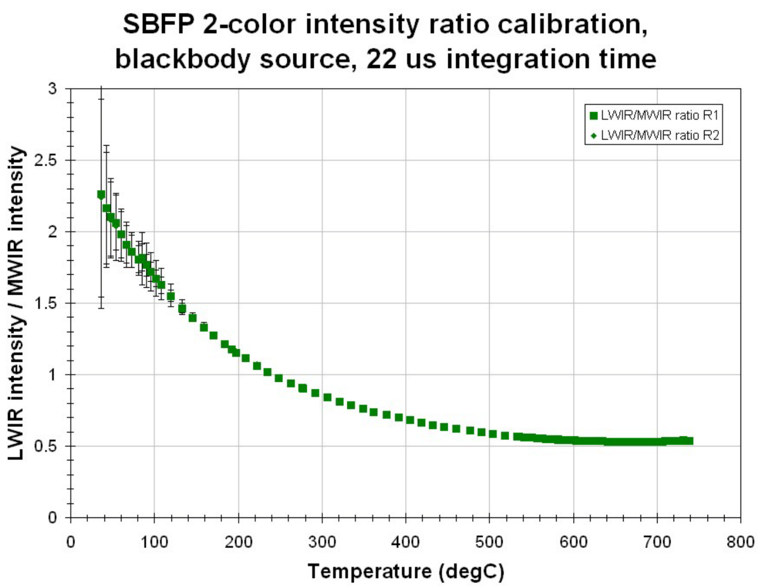

In-situ calibration accomplished during heating of the LLD

- Data captured with dual-band camera viewing LLD plates at 20-320˚C
  - Each LLD plate contains 20 thermocouples embedded in their copper substrate, 5 of which are in positions in the view of the fast IR camera
  - Nearly 500 frames of data taken with 10-75 μs integration time for complete comparison to *ex-situ* calibration data
  - Signal in MWIR band (4-6 μm) reduced by 35-45% due to lack of AR-coating for this spectral band on ZnSe port window, plus dust/dirt/deposits
  - Signal in LWIR band (7-10 μm) also reduced 20-25% likely due to dust/dirt/deposits
  - Overall ~20% increase in LWIR/MWIR ratio compared to *ex-situ* data

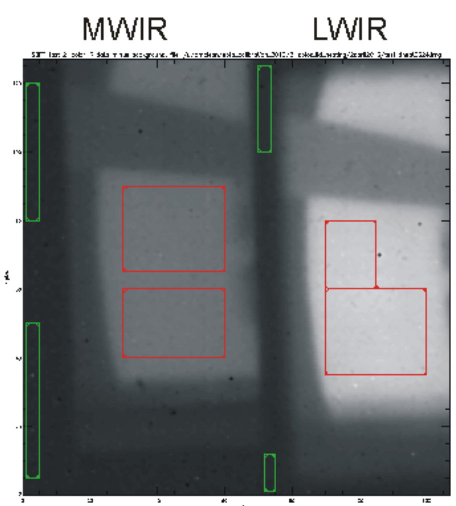

April 2, 2010 12:46.06 PM
Both LLD plates at ~60°C, ratio=2.2

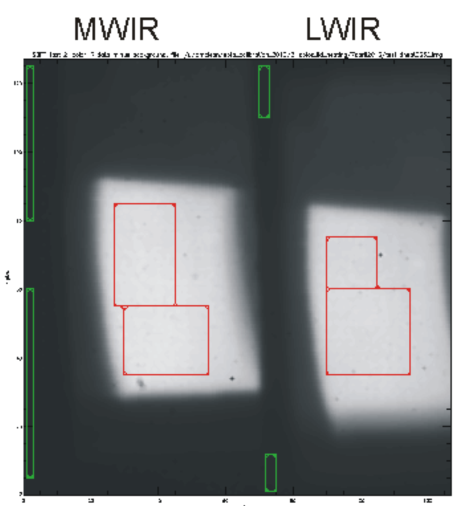

April 7, 2010 3:25.26 PM
K-H LLD plate at ~320°C, ratio=1.0

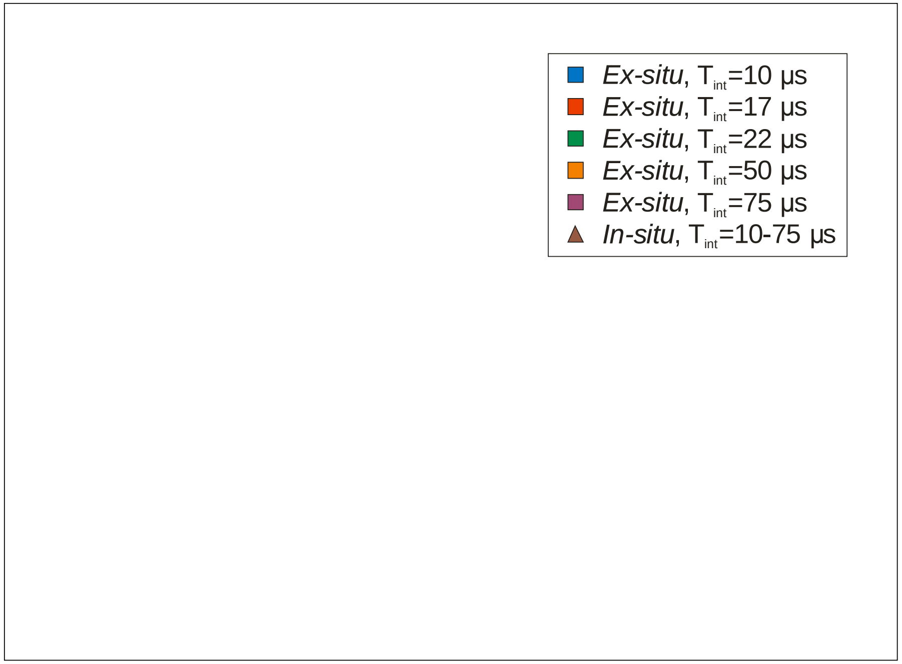

Dual-band IR technique demonstrated on images taken during plasma operation in NSTX with heated LLD

- *Ex-situ* calibration data of T vs. LWIR/MWIR ratio fitted polynomial function, then shifted for best fit to available *in-situ* data
- Data captured in ~350 shots so far, stored to NSTX data acquisition system
- Maximum 128x64 pixels on IR detector per channel (i.e., band), 1.6 kHz frame rate
- In practice, limited to ~45-55 x 100-110 pixels to prevent channel overlap, and allow adequate background for subtraction
- Data analyzed, temperature calibration applied using custom-designed IDL-based software

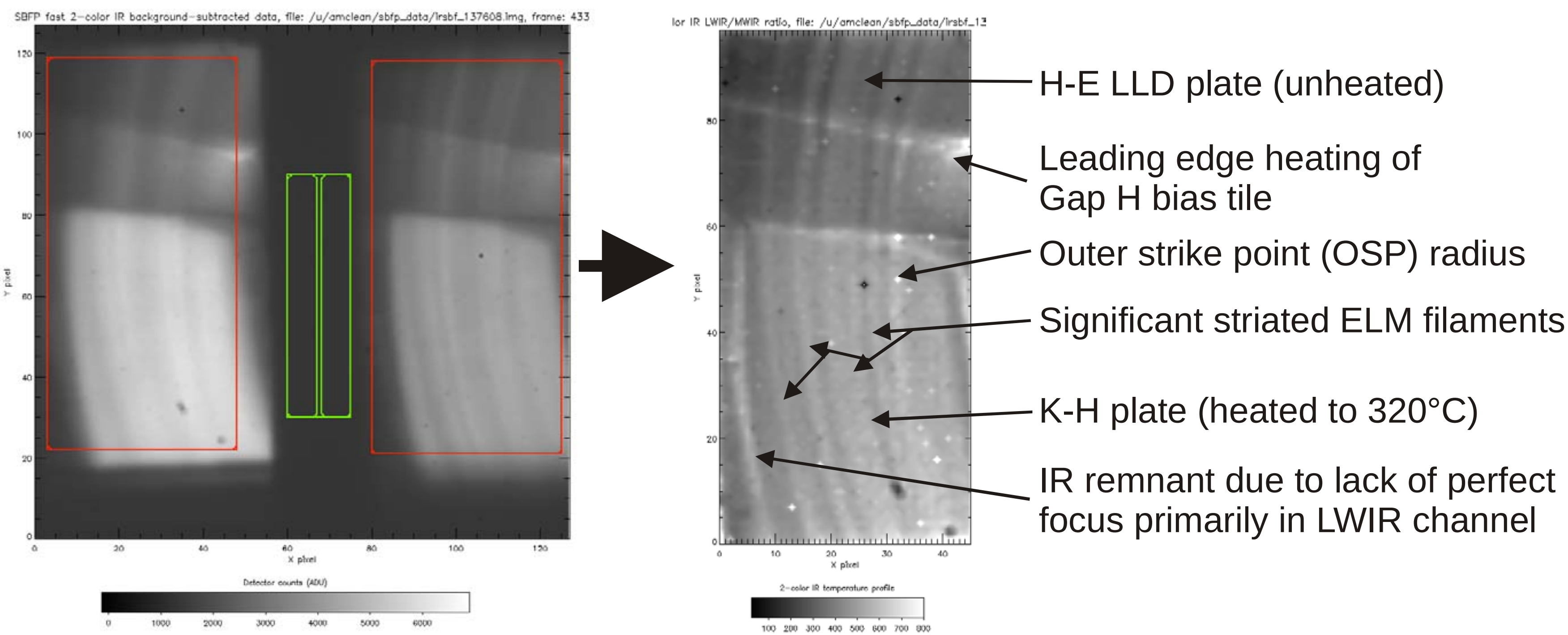

Two-color, wide-angle optical relay design

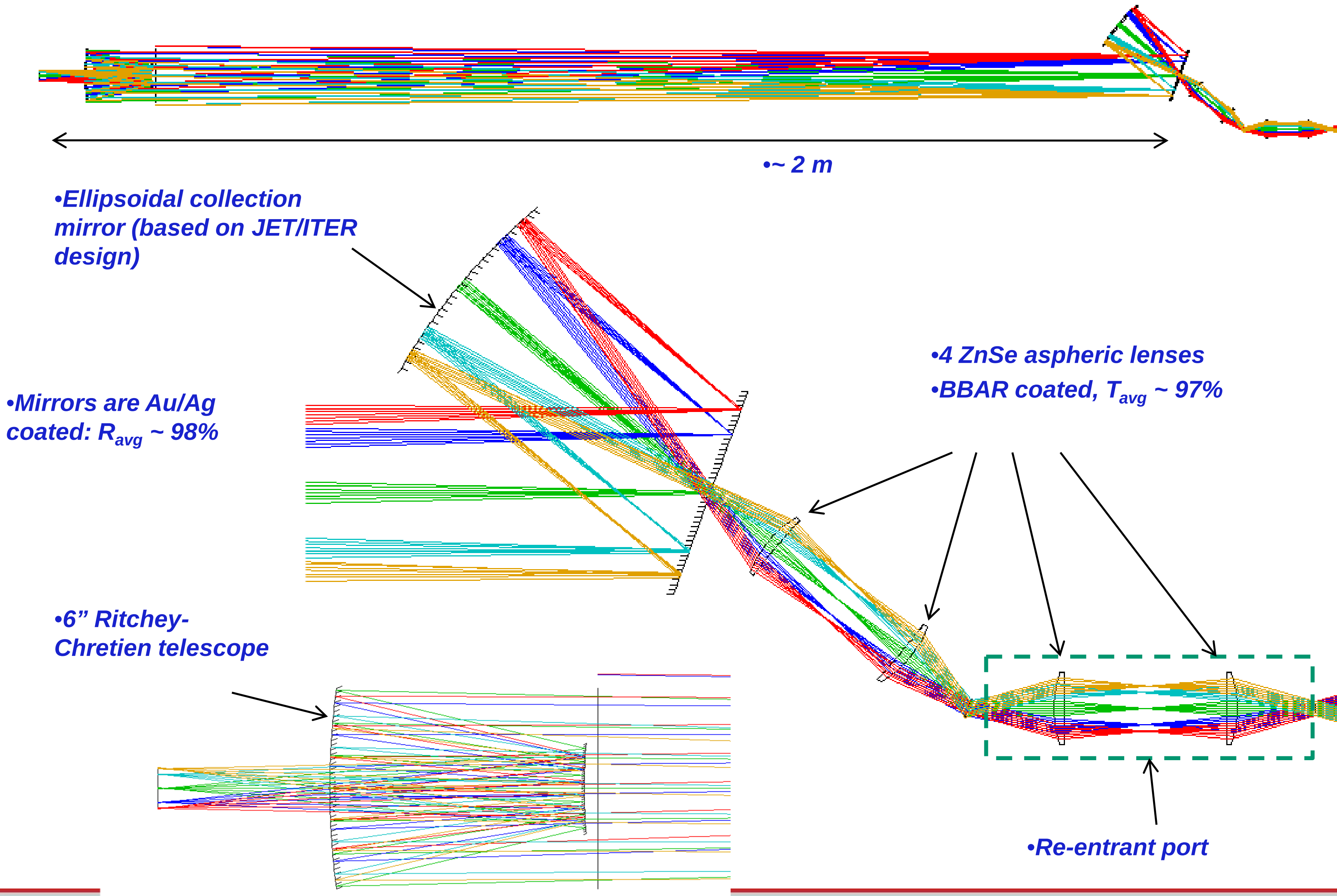

Conclusions

- Dual-band infrared measurement works as expected
- Dual-band system for the ORNL fast IR camera on NSTX successfully designed, built, calibrated and demonstrated
  - Patent pending
- Components <15% of the cost of new dual-band IR camera, and does not limit the full frame-rate capability to ≤300 Hz
- Significant improvements in optical transmission and reduced chromatic aberrations will take place in short term
- Will be used extensively for 1-D and 2-D heat flux measurements on LLD and lithium-coated graphite floor of NSTX
- Dual-band adaptor may be easily optimized for SWIR/MWIR, or dual-color operation within the MWIR or LWIR bands
  - System allows interchange of beamsplitter and IR filters
  - Direct application to existing IR cameras at other fusion facilities (e.g., InSb camera with 3-4 and 4.5-5 μm colors, microbolometer camera with 8-10 and 10.5-12 μm wavelengths)

Future plans

- Mini IR source to allow alignment/focus of system at Bay H port
  - PCMCIA CameraLink card, W-filament and LED IR sources
- Broadband (BB) anti-reflection (AR) coated ZnSe window for port
  - >95% transmission from 3-11 μm would significantly improve dual-band SNR
- Optical relay
  - Makes shielding of the camera against EMF interference, and neutron/gamma radiation possible
  - Extremely challenging for broadband IR (4-10 μm) due to chromatic aberrations
  - Investigating use of reflective optic design similar to JET/ITER design
- Stepper-motor control of Bay H mirror orientation
  - Difficult to properly aim without *in-situ* IR source (heatable tile in 2011)
- Moveable in-vessel protected mirror or IR fiber for window calibration with ex-situ IR source
  - UHV rotary feedthrough bakeable to 350°C (Lesker)
  - IR optical fiber limited to ~300˚C before devitrification